This is a preprint, the final version is subject to change, of the American Mineralogist (MSA)
Cite as Authors (Year) Title. American Mineralogist, in press.
(DOI will not work until issue is live.) DOI: http://dx.doi.org/10.2138/am-2016-5655

Revision 1

Fluorapatite-monazite-allanite relations in the Grängesberg apatite-iron oxide ore district, Bergslagen, Sweden

Erik Jonsson[1,2], Daniel E. Harlov[3,4], Jarosław Majka[1,5], Karin Högdahl[1,6], Katarina Persson-Nilsson[2]

[1]Department of Earth Sciences, Uppsala University, Villavägen 16, SE-75266 Uppsala, Sweden

[2]Geological Survey of Sweden, Department of Mineral Resources, Box 670, SE-75128 Uppsala, Sweden

[3]Section 3.3, Deutsches GeoForschungsZentrum, Telegrafenberg, 14473 Potsdam, Germany

[4]Department of Geology, University of Johannesburg P.O. Box 524, Auckland Park, 2006 South Africa

[5]Faculty of Geology, Geophysics and Environmental Protection, AGH – University of Science and Technology, al. Mickiewicza 30, 30-059 Kraków, Poland

[6]Åbo Akademi University, Department of Geology and Mineralogy, Åbo, Finland

Abstract

Fluorapatite-monazite-xenotime-allanite mineralogy, petrology, and textures are described for a suite of Kiruna-type apatite-iron oxide ore bodies from the Grängesberg Mining District in the Bergslagen ore province, south central Sweden. Fluorapatite occurs in three main lithological assemblages. These include: 1) the apatite-iron oxide ore bodies, 2) breccias associated with the ore bodies, which contain fragmented fluorapatite crystals, and 3) the variably altered host rocks, which contain sporadic, isolated fluorapatite grains or aggregates that are occasionally associated with magnetite in the silicate mineral matrix. Fluorapatite associated with the ore bodies is often zoned, with the outer rim enriched in Y+REE compared to the inner core. It contains sparse monazite

inclusions. In the breccia, fluorapatite is rich in monazite-(Ce) +/- xenotime-(Y) inclusions, especially in its cores, along with reworked, larger monazite grains along fluorapatite and other mineral grain rims. In the host rocks, a small subset of the fluorapatite grains contain monazite +/- xenotime inclusions, while the large majority are devoid of inclusions. Overall, these monazites are relatively poor in Th and U. Allanite-(Ce) is found as inclusions and crack fillings in the fluorapatite from all three assemblage types as well as in the form of independent grains in the surrounding silicate mineral matrix in the host rocks. The apatite-iron oxide ore bodies are proposed to have an igneous, sub-volcanic origin, potentially accompanied by explosive eruptions, which were responsible for the accompanying fluorapatite-rich breccias. Metasomatic alteration of the ore bodies probably began during the later stages of crystallization from residual, magmatically derived HCl- and H_2SO_4-bearing fluids present along grain boundaries. This was most likely followed by fluid exchange between the ore and its host rocks, both immediately after emplacement of the apatite-iron oxide body, and during subsequent phases of regional metamorphism and deformation.

Keywords: fluorapatite, monazite, xenotime, allanite, magnetite, REE, Kiruna-type

Introduction

Apatite-iron oxide ores of the Kiruna type are the single biggest source of iron in Europe (e.g. Islamovic et al., 2015). These large, high-grade, apatite-iron oxide deposits occur worldwide and are generally associated with volcanic to subvolcanic rocks. Notable examples of Kiruna-type deposits include: 1) the Kiirunavaara (Kiruna) ore body, northern Sweden (Geijer, 1910, 1931, 1967; Frietsch, 1978, 1984; Nyström and Henriquez, 1994; Frietsch and Perdahl, 1995; Harlov et al., 2002a; Nyström et al., 2008), 2) the Grängesberg district in south central Sweden (Johansson, 1910; Looström, 1929; Magnusson, 1938; Geijer and Magnusson 1944; Allen et al., 1996; Hitzman et al., 1992; Jonsson et al., 2013), 3) the Mineville ore body, Adirondacks, New York, USA (McKeown and Klemc, 1956; Lupulescu and Pyle, 2005, 2008), 4) the Pea Ridge ore body,

This is a preprint, the final version is subject to change, of the American Mineralogist (MSA)
Cite as Authors (Year) Title. American Mineralogist, in press.
(DOI will not work until issue is live.) DOI: http://dx.doi.org/10.2138/am-2016-5655

Arkansas, USA (Kisvarsanyi and Kisvarsanyi, 1989; Marikos et al., 1989; Sidder et al., 1993; Kerr, 1998; Harlov et al., 2016), 5) a series of ore bodies in the Bafq Region, central Iran (Förster and Jafarzadeh, 1994; Mücke and Younessi, 1994; Daliran, 1990, 2002; Jami et al., 2007; Torab and Lehmann, 2007; Daliran et al., 2010; Bonyadi et al., 2011; Stosch et al., 2011; Taghipour et al., 2015), 6) the Jurassic Marcona deposit in south-central Peru (Chen et al., 2010), 7) the Aoshan fluorapatite-magnetite deposit in the middle-lower Changjiang metallogenic belt, China (Pan and Dong, 1999), and 8) a suite of magnetite-fluorapatite bodies associated with the Plio-Pleistocene volcanoes in the Chilean High Andes and along the Cretaceous Coastal Andean Cordillera, among which is the well-known El Laco deposit (e.g., Nyström and Henriquez, 1989, 1994; Treloar and Colley, 1996; Broman et al., 1999; Naslund et al., 2000, 2002; Henriquez et al., 2003). Beginning with Hitzman et al. (1992), apatite-iron oxide deposits of the Kiruna type, including Grängesberg, were suggested to be related to an "iron oxide (Cu-U-Au-REE)" group of deposits, which were later re-branded as iron oxide copper-gold (IOCG) deposits. This, as has been shown by several workers, is a problematic classification, since most apatite-iron oxide ore deposits contain very little copper or gold (cf. Williams et al., 2005).

Historically, one major hypothesis for the formation of Kiruna-type ores has been that they have an igneous or orthomagmatic origin (Frietsch, 1978). In its present adaptation, this hypothesis suggests that these deposits represent evolved, late stage, igneous bodies, primarily associated with volcanic to sub-volcanic systems, which have experienced a series of metasomatic events ranging from light to intense. These metasomatic events are thought to begin as early as during the later stages of crystallization and continue, either continuously or discontinuously, down to relatively low metamorphic grade (see discussion in Harlov et al., 2002a; 2016). In a number of these occurrences, monazite-(Ce) +/- xenotime-(Y) are commonly found associated as inclusions or rim grains with apatite that has experienced fluid-induced alteration in the form of (Y+REE) + Na + Si + Cl depletion, e.g. at Kiirunavaara in northern Sweden (Harlov et al., 2002a) or Bafq in central Iran (Torab and Lehmann, 2007), with the fluorapatite acting as the source of P and (Y+REE) for

the newly formed monazite and xenotime (Harlov et al., 2002b; Harlov and Förster, 2003; Harlov et al., 2005).

The apatite-iron oxide deposits of the Grängesberg-Blötberget-Idkerberget mining districts are situated in the Palaeoproterozoic Bergslagen ore province in central Sweden (Fig. 1). Besides being the largest concentration of iron oxide ore in southern and central Sweden, these deposits also represent a possible future economic source of REE and P (Hallberg and Jonsson, 2006; Jonsson et al., 2010a, b; Goodenough et al., 2016). During the inception of large-scale mining in the early 1900s, the Grängesberg deposits were already being compared to those of the Kiruna District in northernmost Sweden (Johansson, 1910; Looström, 1929, 1939; Magnusson, 1970). The discussion concerning the origin of these ores has continued up to the present day (e.g. Hitzman et al., 1992; Jonsson et al., 2013). Based on the mineralogy, deposit geometry, relations to host rocks, and overall geochemical character, the most likely explanation is that the apatite-iron oxide ores in the Grängesberg District represent deformed and metamorphosed, Palaeoproterozoic Kiruna-type deposits (Jonsson et al., 2010a). Evidence from oxygen and Fe isotope systematics as well as geochemistry furthermore suggests a primarily orthomagmatic mode of iron oxide formation with localized hydrothermal alteration (Jonsson et al., 2013; Weis et al., 2013).

In this study, we document REE-mineral textures and assemblages in a suite of magnetite-fluorapatite-silicate associations from Grängesberg and surrounding locations, based on 21 samples from both existing outcrops, including the Fallgruvan mine, and drill-cores transecting the main ore zone in the central part of the Grängesberg District, the so-called Export field (Fig 1). The first aim of this study is to document and characterize fluorapatite-monazite (±xenotime)-allanite relations in the apatite-iron oxide ores from the Grängesberg deposit. A second, and equally important, aim is to explore how fluid-aided alteration relates to the formation of monazite and xenotime inclusions in the fluorapatite and the later remobilization of (Y+REE) outside of the fluorapatite into the surrounding mineral matrix. This allows us to constrain the probable chemistry and activity of these

This is a preprint, the final version is subject to change, of the American Mineralogist (MSA)
Cite as Authors (Year) Title. American Mineralogist, in press.
(DOI will not work until issue is live.) DOI: http://dx.doi.org/10.2138/am-2016-5655

fluids, as well as attempt to unravel the temporal relationships between variable and chemically different fluid fluxes.

Geological Background

The Bergslagen ore province is an intensely mineralized area that comprises the southernmost part of the Palaeoproterozoic Svecokarelian orogen in south central Sweden (Fig. 1). The province contains a multitude of ore types, dominated by base metal mineralization and Fe oxide ores (e.g. Tegengren, 1924; Geijer and Magnusson, 1944; Magnusson, 1938, 1970; Stephens et al., 2009). The main ore-bearing, meta-supracrustal sequence is dominated by felsic, alkali-enriched metavolcanic rocks, different types of metabasic rocks, clastic metasedimentary rocks, and calcitic to dolomitic marbles. This rock association is thought to have formed at c. 1.90-1.87 Ga during volcanism in a shallow marine, continental back-arc setting (Allen et al., 1996; Stephens et al., 2009, and references therein). Mineralization occurs primarily in rhyolitic to dacitic metavolcanic rock units, including commonly interlayered marbles and skarns. The latter, variably Fe-, Mg-, and/or Mn-bearing calc-silicate assemblages, occur as two main genetic types, which either formed as a consequence of regional metamorphism of impure carbonate rocks, or through metasomatic reactions between felsic magmatic-derived, silica-rich fluids and pre-existing carbonate rocks.

All major rock units in the western part of the Bergslagen ore province, except the youngest granitic intrusives and dolerites, have been affected by regional (Svecokarelian) metamorphism, which reached low pressure, high temperature greenschist- to amphibolite-facies grade (cf. Stephens et al., 2009, and references therein). The regional metamorphism in south central Sweden is most likely polyphase, and is constrained to the c. 1.87 – 1.80 Ga time interval (e.g. Andersson, 1997; Hermansson et al., 2007; Stephens et al., 2009). In the early orogenic rocks in the Grängesberg area, amphibolite-facies conditions prevail.

The host rocks immediate to the Grängesberg ores exhibit significantly more intermediate to mafic compositions compared to the overall felsic character of the metavolcanic rocks elsewhere in

the Bergslagen province (Fig. 1). The dominating rocks in the main ore zone of Grängesberg, (referred to as the Export field), are variable feldspar-porphyric meta-dacites to meta-andesites, whereas meta-rhyolites are subordinate. Surrounding the Export field there are different types of breccias, including syn-volcanic fragmented rocks, a fluorapatite breccia, and a breccia with a magnetite-rich matrix (e.g. Högdahl et al., 2013). Crosscutting, subvolcanic dykes of variable compositions are ubiquitous not least in and around the Export field. Intrusive rocks are represented by a c. 1895 Ma gneissic granodiorite, which is located in the hanging wall, i.e. east of the main ore zone, and a metagranite and associated pegmatites in the footwall to the west (Fig. 1; Högdahl et al., 2013).

Alteration is evident in the metavolcanic host rock, both in the form of regional-style Na or K alteration, and locally, as Mg +/- K alteration in the form of disseminations as well as discrete zones rich in phyllosilicates (mainly biotite + chlorite) and calcic Mg-Fe-clinoamphiboles classified as either hornblende and actinolite (cf. Leake et al., 1997), which locally known as sköl zones (Fig. 1). Furthermore, localized, large-scale alteration of the hanging-wall host rocks into partly fluorite-bearing, biotite-chlorite-(clinoamphibole-magnetite-fluorapatite)-dominated assemblages was documented from the Export field during mining by N. H. Magnusson (cf. Geijer and Magnusson, 1944).

Three ductile deformation phases (D1-D3) have been recognized in the Grängesberg District, which has later been subjected to brittle deformation along localized deformation zones (Högdahl et al., 2013). The oldest structure is a crenulated foliation related to up-right, isoclinal F1-folds. These folds were subsequently deformed under peak-metamorphic conditions during the D2 phase, when the structures formed were controlled by the competence contrasts between the various rock types. The iron oxide bodies and the metagranitoids to the east and west acted as a rigid bodies and strain was mainly accommodated in the altered rocks, including the sköl zones. These rocks have a penetrative foliation, a strong, steep stretching lineation that is parallel to the fold axis of the

local, double plunging F2-folds, whereas the competent rocks formed boudins. Open, large-scale F3-folds formed later under retrograde conditions (cf. Högdahl et al., 2013).

Grängesberg apatite-iron oxide ore types and assemblages

The apatite-iron oxide deposits of the Grängesberg District (past production 152 Mt of ore with 58% Fe and 0.81% P) comprise the single biggest concentration of iron ore in the Bergslagen province, and thus in all of central and southern Sweden (Hallberg and Jonsson, 2006; Fig. 1). These deposits, and their NNW continuation via Blötberget to Idkerberget, constitute both a geological as well as an ore genetic anomaly in the province. In Bergslagen, several thousand Fe oxide deposits are known to exist (based on SGU databases). However, all, but those in the Grängesberg-Blötberget-Idkerberget districts, are either hematite-dominated, quartz-rich ores, typically banded iron formations, or magnetite-dominated skarn-type deposits.

The Grängesberg District Fe oxide ores range from magnetite to hematite-dominated (Figs. 1 and 2). They are variably rich in fluorapatite and accessory silicate minerals, which include amphibole, biotite, and chlorite. Overall, the Export field at Grängesberg has been estimated to consist of about 80% magnetite ore and 20% hematite ore (e.g. Jonsson et al., 2011). The ore occurs as a north-north-east trending lens-like system dipping moderately to steeply towards the east. Within this roughly planar system, the individual ore bodies have been described as “log-shaped bodies” (Geijer and Magnusson, 1944), due to deformation associated with D2 (Högdahl et al., 2013). The hematite-rich ores are concentrated towards the structural footwall on the west, with the main magnetite-ore occurring in the central part and towards the east.

The two ore types are generally dominated by one oxide mineral, although the hematite ores often exhibit an intermixed magnetite component (Table 1; Fig. 2a-d). It is not uncommon to observe magnetite blastesis in massive, fine-grained hematite ores. These magnetite porphyroblasts are often large and euhedral to subhedral, which indicates growth under comparatively strain-free conditions. Even though banded zones with magnetite veins in the hematite ore have also been

This is a preprint, the final version is subject to change, of the American Mineralogist (MSA)
Cite as Authors (Year) Title. American Mineralogist, in press.
(DOI will not work until issue is live.) DOI: http://dx.doi.org/10.2138/am-2016-5655

encountered, the transition between the hematite and magnetite ores is often rather sharp. A transition zone with varying proportions of magnetite and hematite occur, typically in the vicinity of crosscutting pegmatites. However, this has also been described from other parts of the mine (e.g. Geijer and Magnusson, 1944), demonstrating that this process is not solely attributed to the intrusion of pegmatites.

The magnetite ores are often fine to medium-grained, massive, and frequently with a distinct "grainy" appearance in hand specimen, and a "foamy" or granoblastic microtexture (Figs. 2a,b,c). Much of the hematite-dominated ores consist of massive, fine to medium-grained, often platy hematite (Fig. 2d). Almost all ore types show a variable degree of banding, with the lighter bands dominated by fine-grained aggregates of fluorapatite and accessory silicates (Figs. 2d). This banding is considered to be primary, although an enhancement of the planar structure, due to later deformation, is observed in many samples. Together with the surrounding host rocks, magnetite, hematite, fluorapatite, and associated subordinate minerals in the ore bodies were affected during regional metamorphism. However, a partially preserved magmatic texture is supported by the behavior of the larger iron oxide ore bodies in the Export field during Svecokarelian ductile deformation at peak metamorphic conditions. Here, the competence contrast caused strain partitioning leading to a strong fabric in the less competent immediate host rocks and sköl zones, and mega-boudin-formation (the "log-shaped bodies" of Geijer and Magnusson, 1944) of the rigid ore bodies, which therefore mainly escaped penetrative deformation (Högdahl et al. 2013; Persson-Nilsson et al. 2013). Strain was also accommodated by the sköl zones within the apatite-iron oxide ores and to a lesser degree by the bands of apatite and accessory silicates. However, static metamorphic recrystallization of the ores and the fluorapatite ± silicate assemblages cannot be completely ruled out (Jonsson et al. 2010b).

REE in the ores are mainly hosted by the granular fluorapatite, which is typically high in Y, Ce, La, and Nd (Fig. 3). However, they are also present in phases that occur in texturally later-formed positions, mainly monazite-(Ce), xenotime-(Y), allanite-(Ce), and REE-bearing epidote

This is a preprint, the final version is subject to change, of the American Mineralogist (MSA)
Cite as Authors (Year) Title. American Mineralogist, in press.
(DOI will not work until issue is live.) DOI: http://dx.doi.org/10.2138/am-2016-5655

(Figs. 4 and 5). At a later stage, LREE-fluorocarbonate(s) formed during low-temperature remobilization of the REEs. Within the surrounding host rocks, REEs are concentrated in allanite, fluorapatite, and monazite (Jonsson et al., 2010b).

Field relations in the northern part of the Grängesberg District (Fig. 1) indicate that the ore formation pre-dates emplacement of the 1895 Ma granodiorite, which hosts similar apatite-iron oxide mineralization in the form of variably-sized xenoliths (Jonsson et al., 2011; Högdahl et al., 2013). The recent discovery of numerous angular fluorapatite fragments occurring in discrete horizons (i.e. volcanic breccias) within the metavolcanic rock of the structural footwall to the ore zone is of major importance, as it implies that fragments of an already crystallized massive fluorapatite assemblage were being erupted. Thus, formation of at least part of the iron oxide-fluorapatite system was either coeval with, or pre-dated these volcanic units (Jonsson et al., 2011).

Analytical Techniques

Textural relationships between minerals were examined at the Deutsches GeoForschungsZentrum, Potsdam using high contrast back scattered electron (BSE) imaging on a Zeiss DSM-962 Scanning Electron Microscope (1 μm electron beam spot; 15 or 20 kV).

Electron microprobe (EMP) analyses were carried out using a Cameca SX100 electron microprobe at the Deutsches GeoForschungsZentrum. Analyses of fluorapatite were performed at 10 kV and 10 nA using a defocused 20 μm diameter beam spot. The REE in fluorapatite were measured separately using an acceleration voltage of 20 kV and a beam current of 20 nA. Monazite was analyzed with an acceleration voltage of 20 kV, a beam current of 40 nA and a beam diameter of 1 μm. Allanite was analyzed with an acceleration voltage of 20 kV, a beam current of 20 nA, and a beam diameter of 1 μm.

Fluorapatite grains, analyzed using EMP, were first examined in BSE mode and only those areas free of monazite inclusions were chosen for analysis. With the exception of F, the fluorapatite analyses listed in Table 2 represent an average of between 4 to 11 grains evenly scattered over the

This is a preprint, the final version is subject to change, of the American Mineralogist (MSA)
Cite as Authors (Year) Title. American Mineralogist, in press.
(DOI will not work until issue is live.) DOI: http://dx.doi.org/10.2138/am-2016-5655

thin section. Since F X-ray excitation tends to increase with time during EMP analysis (Stormer et al., 1993), the F value from the fluorapatite grain in each sample with the lowest F concentration was chosen as the representative value for F for the corresponding mean fluorapatite analysis listed in Table 2 for that sample. Whenever possible, elongated fluorapatite grains approximately parallel to [0001] were chosen for analysis since this minimizes the increase in F X-ray excitation with time during EMP analysis (Stormer et al., 1993; Pyle et al., 2002; Goldoff et al., 2012). The hydroxyl content was estimated utilizing charge balance with F and Cl on the anion site.

Silicate, oxide, and metal standards were taken from both the CAMECA and Smithsonian standard sets (Jarosewich et al., 1980). Standards for the REE were taken from a set of synthetic REE phosphates prepared by Jarosewich and Boatner (1991). The Cameca PAP program was used for matrix correction (Pouchou and Pichoir, 1985). Relative errors in EMP analyses are estimated to be < 1% at the > 10 oxide wt% level, 5 − 10% at the 1 oxide wt% level, 10 − 20% at the 0.2 to 1 oxide wt% level, and 20 − 40% at the < 0.1 oxide wt% level. Detection limits were approximately 500 ppm for the (Y + REE), and 200 – 300 ppm for Th and U.

The full data set representing all analyses are provided as electronic supplementary material (fluorapatite: Appendix A; monazite (and xenotime): Appendix B; allanite: Appendix C) from the American Mineralogist website.

REE-bearing minerals, their chemistry and textural context

The 21 samples covered in this study comprise three different main lithologies, or assemblage types (Table 1). These include (1) the magnetite-fluorapatite and hematite-magnetite-fluorapatite ore grade bodies (apatite-iron oxide ores); (2) the associated metavolcanic-hosted, fluorapatite-bearing breccias (breccias); and (3) the variably altered and fluorapatite ± iron oxide-bearing metavolcanic host rocks (host rocks), including the poly-deformed, phyllosilicate ± amphibole-rich alteration assemblages present in the sköl rocks. All three lithologies also host monazite-(Ce), xenotime-(Y), and allanite-(Ce) in varying amounts.

This is a preprint, the final version is subject to change, of the American Mineralogist (MSA)
Cite as Authors (Year) Title. American Mineralogist, in press.
(DOI will not work until issue is live.) DOI: http://dx.doi.org/10.2138/am-2016-5655

High-resolution BSE imaging revealed that the fluorapatite occurs as two main textural types, of which one is found only in the apatite-iron oxide ore bodies (Type 1 assemblage). This fluorapatite exhibits variably extensive, concentric zoning (Fig. 3), usually with BSE-darker cores that becomes increasingly lighter towards the rims and ends with a BSE-dark outermost thin rim. This trend is rarely reversed. Light zones are highly enriched in Y+REE (up to 2.5 wt.% total $(Y+REE)_2O_3$ and SiO_2; Table 2) relative to the dark zones. Rare, tiny (< 5 μm), scattered monazite (± xenotime) inclusions are present in the BSE-dark zones. In some cases, the monazite (± xenotime) inclusions are elongated parallel to the fluorapatite c-axis in a topotaxial relationship (cf. Pan et al., 1993; Figs. 3c, 4a,b).

The other textural variety is found both in the breccias (Type 2 assemblage) and in the host rocks (Type 3 assemblage). In the breccia the fluorapatite consists mainly of coarse, angular fragments and crystals, whereas in the host rocks it tends to occur as isolated, subhedral to euhedral grains. In either assemblage type, the fluorapatite is unzoned and generally (Y+REE)-poor. It characteristically contains variable amounts of monazite (± xenotime) inclusions ranging from scattered to very numerous (Fig. 4). These are concentrated in the cores of the fluorapatite, whereas the rims commonly lack inclusions. The inclusions range in size from < 1 micron to several tens of microns in size. Monazite grains of this size and larger can also occur outside of the fluorapatite. In all three assemblage types, the relative abundances of Si and (Y+REE) in fluorapatite show a distinct correlation, as opposed to Na and (Y+REE) (see discussion in Harlov et al., 2002b). This relationship can principally be expressed in the form of the following coupled substitution reaction (Fig. 6; Pan and Fleet 2002): $Si^{4+} + (Y+REE)^{3+} = P^{5+} + Ca^{2+}$.

Regardless of assemblage type, or whether occurring as an inclusion in fluorapatite, or as a free grain in the surrounding mineral matrix, the monazite is Ce-dominant, with the a ThO_2 content not exceeding 1 wt% in the main ore zone, though it can reach up to 2.1 wt% in Fallgruvan (Fig. 1; Table 1). In addition, Y_2O_3 values are significantly lower (up to 0.48 wt%) than those at Fallgruvan (up to 2.10 wt%; Table 3). Taking into account the presence of co-existing xenotime, the low Y

This is a preprint, the final version is subject to change, of the American Mineralogist (MSA)
Cite as Authors (Year) Title. American Mineralogist, in press.
(DOI will not work until issue is live.) DOI: http://dx.doi.org/10.2138/am-2016-5655

contents in monazite imply formation temperatures, of 300 °C or less, utilizing the monazite-xenotime geothermometer of Gratz and Heinrich (1997) and Heinrich et al. (1997). This suggests that the metasomatic event or events responsible for the nucleation and growth of monazite +/- xenotime from fluorapatite occurred at relatively low temperatures. The SiO_2 content in all monazites does not exceed 0.76 wt%, whereas the CaO values range between 0.21 and 2.38 wt% (Table 3), indicating that both the huttonite ($ThSiO_4$) and cheralite ($ThCa(PO_4)_2$) substitutions are limited (Förster, 1998). Monazite (and xenotime) with low Th contents, associated with fluorapatite as inclusions and as rim grains, have previously been described from other fluorapatite-iron oxide ore deposits, including Kiirunavaara (Harlov et al. 2002a), Pea Ridge (Kerr, 1998; Harlov et al., 2016), Bafq (Torab and Lehman, 2007; Taghipour et al., 2015), and Mineville (Lupulescu and Pyle, 2008).

Allanite-(Ce) is found in all three assemblage types. It occurs within fluorapatite as inclusions or along cracks, along fluorapatite and other mineral grain boundaries (Fig. 5a,b,c), and as large composite grains in the surrounding silicate mineral matrix of the host rocks, often associated with what appears to be recrystallized magnetite (Fig. 5d). The allanite grains are often complexly zoned. In the breccias (Type 2 assemblage), the abundance and size of the allanite inclusions appears to increase towards the edges and immediately outside of the fluorapatite fragments. In the host rocks (Type 3 assemblage), allanite commonly occurs as interstitial grains in the iron oxide-fluorapatite bands as well as in the form of subhedral grains and aggregates dispersed in the groundmass (Fig. 5). In all the samples, the allanite contains minor amounts of MgO (Table 4). Thorium concentrations are very low and range from below the EMP detection limit to 0.75 wt% ThO_2 , whereas U concentrations are close to or below the EMP detection limit.

This is a preprint, the final version is subject to change, of the American Mineralogist (MSA)
Cite as Authors (Year) Title. American Mineralogist, in press.
(DOI will not work until issue is live.) DOI: http://dx.doi.org/10.2138/am-2016-5655

Discussion

Monazite-xenotime-fluorapatite microtextures and associated fluid activity

It has been demonstrated experimentally that the formation of monazite (±xenotime) inclusions in fluorapatite is a fluid-induced process, which occurs as a result of coupled dissolution-reprecipitation (Harlov and Förster, 2003; Harlov et al., 2005; Putnis, 2009; Putnis and Austrheim, 2012). When this process occurred in the Grängesberg apatite-iron oxide ores, breccias, and host rocks is a matter of some conjecture. This first of all assumes that the ores represent the end-products of late stage, highly evolved iron oxide-fluorapatite melts formed in a sub-volcanic setting. This seems to be supported by both the interpretation of the field evidence per the description of the Grängesberg Deposit in general (see above), and it is consistent with stable isotope systematics (Jonsson et al., 2013; Weis et al., 2013). The magmatic scenario is also supported by the intimate association of apatite-iron oxide deposits with Plio-Pleistocene volcanoes from the Chilean High Andes and along the Cretaceous Coastal Andean Cordillera, along with many of their internal features (Nyström and Henriquez, 1989, 1994; Broman et al., 1999; Naslund et al., 2000, 2002; Henriquez et al., 2003; Knipping et al., 2015). Also, the Cl/Br values of fluorapatite from the Aoshan fluorapatite-magnetite deposit are compatible with an orthomagmatic origin (Dong, 2005).

Assuming that the Grängesberg ore bodies originated as high-temperature iron oxide magmas emplaced in a thick, still forming, mainly submarine volcano-sedimentary pile (cf. Allen et al., 1996), it is very likely that any existing fluids (remnant seawater, pore waters, formation waters) in these units would have been mobilized during this process. These fluids, along with the probable presence of volatiles released during the crystallization of the iron oxide-fluorapatite bodies, would have allowed for a late to post-magmatic hydrothermal system to have formed around the ore zone. This would have led to “secondary” alteration and mineralizing processes within the ore bodies and their surrounding host rocks, as also attested by field observations. The initial fluid-mediated alteration that took place either immediately after, or during the later stages of crystallization of the iron oxide ore, is likely to have been primarily due to the acidic fluids that were expelled by the

cooling magma, i.e., an auto-metasomatic alteration. Post-dating the magmatic stage, fluids associated with the regional metamorphism affecting the western part of the Bergslagen province could later also have affected the apatite-iron oxide ores and their host rocks. In addition, the occurrence of REE-fluorocarbonates as a minor component in the ore assemblages indicates that small-scale REE remobilization occurred at low pressure and temperature conditions, long after peak regional metamorphism.

Experimental studies have demonstrated that H_2O, KCl brines, and H_2O-CO_2 fluids, as well as acids such as HCl and H_2SO_4, will react with fluorapatite, resulting in the formation of monazite +/- xenotime both as inclusions in the fluorapatite and as grains along the fluorapatite grain rim, from the (Y+REE) + P budget at hand (Harlov et al., 2003, 2005). This takes place through a coupled dissolution-reprecipitation process (Putnis, 2009; Putnis and Austrheim, 2012), in which REE phosphate mineral formation is directly associated with the formation of an interconnected micro/nano-porosity within the chemically altered, (Y+REE)-depleted areas of the fluorapatite (Harlov et al., 2005; see also Putnis, 2009). Fluid infiltration within this interconnected nano-porosity promotes fluid-mediated mass transfer of (Y+REE), Si, Na, Ca, and P from the host fluorapatite and the subsequent formation of monazite (± xenotime) inclusions in the nano/micro-pores, which serve as nucleation sites. Once formed, these same fluids, or later ones appear to further induce mobilization of REE and P, which can result in the Ostwald ripening of the monazite and xenotime inclusions in the fluorapatite. This process leads to a decrease in the total number of inclusions, while, at the same time, increasing the size of the remaining ones. In addition, this could also have resulted in the mobilization of REE out of the fluorapatite to form monazite and xenotime, both as grains occurring along the rims of the fluorapatite, as well as independent grains in the surrounding mineral matrix. REE mobilized by similar fluids, which reacted with the surrounding silicate-dominated mineral matrix, resulted in the formation of allanite, whose stability field tends to be at lower pressures and temperatures in the SiO_2-Al_2O_3-Na_2O-K_2O-CaO-H_2O system, compared to that of monazite (e.g. Spear, 2010). This, however, also depends to some

degree on the relative CaO and Na_2O activities in the surrounding silicate host rocks, and subsequently the fluids originating from these rocks (Finger et al., 1998; Janots et al., 2007; 2008; Spear, 2010; Budzyń et al., 2011). In general, the relatively low temperatures (< 300 °C), inferred from Y partitioning between co-existing monazite-(Ce) and xenotime-(Y) as inclusions in fluorapatite, as rim grains on fluorapatite, and as matrix grains (see above; Gratz and Heinrich, 1997; Heinrich et al., 1997) suggests that the formation of monazite-(Ce) and xenotime-(Y), as well as further fluid-mediated remobilization, most likely occurred during post-peak regional metamorphism/metasomatism.

Fluorapatite grain fragments from the breccias (Type 2 assemblages) and fluorapatite grains from altered, silicate-rich host rocks (Type 3 assemblages) contain abundant monazite (± xenotime) inclusions in their interior, but tend to be inclusion-free in the outermost rims (Fig. 4). This suggests that the rims of the fluorapatite crystals were in contact with, and leached by highly reactive fluids migrating along grain boundaries. Tropper et al. (2011, 2013) have shown that (Y+REE) are highly mobile in alkali-bearing F- and Cl-rich fluids, which could have been responsible for the leaching of (Y+REE) from the originally (Y+REE)-enriched rims of the zoned crystals. Simultaneously, this process would encourage the formation of monazite (± xenotime) inclusions in the central regions of the crystals (Harlov and Förster, 2003; Harlov et al., 2005). It is therefore conceivable that these now REE-depleted, reacted fluorapatite rims could have been the source of components for the formation of monazite and xenotime, as well as the allanite grains in the surrounding mineral matrix. These observations allow for reconstruction of a sequence of events that led to the formation of the highly evolved fluorapatite textures observed in the Type 2 and 3 assemblages. The REE-enriched zones in the Type 1 assemblages are possibly the only remnants of a primary texture representing the original, presumably orthomagmatic fluorapatite. This was then successively depleted in REE due to the activity of infiltrating fluids. The inclusion-rich fluorapatite observed in all three assemblages represents a later stage in the fluid-aided evolution of these rocks, whereas

This is a preprint, the final version is subject to change, of the American Mineralogist (MSA)
Cite as Authors (Year) Title. American Mineralogist, in press.
(DOI will not work until issue is live.) DOI: http://dx.doi.org/10.2138/am-2016-5655

inclusion- and REE-free zones (usually rims) were formed during the last stage of metasomatic alteration.

The variably deformed and altered host rocks (Type 3 assemblages) exhibit an even more mature stage of fluid infiltration, during which fluorapatite has been completely leached and only allanite occurs as fracture-fillings within the fluorapatite and as veins and grains in the surrounding mineral matrix (e.g. Fig 5). This last stage of REE mobility is represented by the sparse occurrence of late stage REE-fluorocarbonates, both as isolated aggregates and as replacements of pre-existing REE-rich phases, implying an either internally or externally derived F^- and CO_3^{2-} component in these fluids. The low-temperature mineralogy and the possibility of an externally derived fluid input to these assemblages are in accordance particularly with their appearance in the most intensely deformed and schistose sköl-type host rocks. These are likely to have been multiply overprinted by deformation and metasomatizing fluids after the formation of the iron ore, as well as post-dating regional metamorphism.

Comparison of the Grängesberg apatite-iron oxide ore with other Kiruna-type deposits

The Grängesberg ores share some similarities with the other Kiruna-type iron oxide-apatite ore deposits, especially the *sensu stricto* Kiirunavaara (Kiruna) ores of northern Sweden and those from the Bafq district in Iran (e.g. Whitten and Yancey, 1990; Harlov et al., 2002a; Daliran et al., 2010). In the Kiruna and Bafq deposits, REE-enriched fluorapatites (up to 2–3 wt.% REE_2O_3) with inclusions of monazite and/or xenotime are common (Harlov et al., 2002a; Torab and Lehmann, 2007; Bonyadi et al., 2011; Taghipour et al., 2015). These inclusions are either randomly oriented or, in some cases are elongated along the c-axis of apatite in an topotaxial relationship (Pan et al., 1993). Similar to what is seen in Grängesberg, monazite (both as inclusions in fluorapatite and as separate grains) from these ore bodies is low in Th, with contents not exceeding 2 wt.%, though some monazite grains from the Bafq ore bodies, have Th-enriched cores (see Torab and Lehmann, 2007). In the Kiirunavaara ores, REE zoning patterns in fluorapatite are remarkably similar to what

is seen in the Grängesberg ores. In contrast, the Bafq district fluorapatites exhibit rather patchy zoning patterns (e.g. Bonyadi et al. 2011). This might be due to the more shallow depth of formation, and hence lesser degree of "compaction" of the shallow to extrusive, geologically younger (approx. 550 Ma) Bafq ores (Daliran, 2002; Daliran et al., 2010). This would in turn have allowed for more pore space to be available for late fluid percolation and very likely the formation of lower-temperature REE-bearing fluorapatite. The deeper-formed, more dike-(sill-)like Grängesberg and Kiruna ores would have offered less available pore space allowing fluid to only infiltrate along fractures or grain boundaries. In the latter case, the fluid may thus have reacted predominantly with the outer zones of the fluorapatite grains/crystals during this process.

Alternatively, pre-metamorphic zoning in the Kiruna and Grängesberg deposits may have been, at least in part, obliterated, leaving patterns related to metamorphic recrystallization as well as to late to post-metamorphic fluid percolation. The contrast between the regionally metamorphosed and deformed c. 1.88 – 1.90 Ga Kiruna and Grängesberg ores and younger, better-preserved c. 0.55 Ga Bafq ones could thus be due to the difference in the extent of post-formation modification of the iron ore bodies.

Fluorapatite from well-known apatite-iron oxide ores, such as those at El Laco, Chile (c. 2 Ma; Naranjo et al., 2010; Naslund et al., 2002) or Cerro de Mercado (Durango), Mexico (c. 30 Ma; Boyce and Hodges, 2005), has not been reported to contain inclusions of monazite ± xenotime, though, in the case of Cerro de Mercado, the fluorapatite is known to contain at least several weight percent (Y+REE) (e.g., Young et al. 1969; see also Harlov and Förster, 2003; Harlov et al., 2005). However, these ores share many mineralogical, geochemical, textural, and structural features of Grängesberg. They also formed in similar, tectonically and volcanically active settings in constructional margin environments. In the case of El Laco, a fluid inclusion study of the fluorapatite has documented Cl-bearing, high-salinity fluid activity during crystallization of the flourapatite from the original melt (e.g., Broman et al. 1999, Naranjo et al. 2010).

This is a preprint, the final version is subject to change, of the American Mineralogist (MSA)
Cite as Authors (Year) Title. American Mineralogist, in press.
(DOI will not work until issue is live.) DOI: http://dx.doi.org/10.2138/am-2016-5655

Implications

When comparing the apatite-iron oxide ore body at Grängesberg with other Kiruna-type magnetite-apatite deposits globally (as outlined above), a principal observation is that each of them in some way formed in direct association with concurrent volcanic to sub-volcanic activity. In the cases of both Kiruna and Grängesberg, different types of breccias affecting both ores and volcanic-subvolcanic host rocks are a characteristic element. In some cases, these apatite-iron oxide ore deposits have actually been observed to be associated with active volcanic systems, such as in the case of the El Laco complex in Chile (cf. Nyström and Henriquez, 1989, 1994; Broman et al., 1999; Naslund et al., 2002; Henriquez et al., 2003). This intimate association with volcanic host rocks, both in the distant past (e.g. the Palaeoproterozoic Kiirunavaara and Grängesberg deposits and the Mesoproterozoic Pea Ridge deposits), as well as in more recent formations (the Cambrian Bafq, Jurassic Marcona, and Chilean Plio-Pleistocene deposits) strongly suggest that the apatite-iron oxide ores are magmatic in origin. This is then followed by metasomatic reworking over a long period of time to varying degrees, depending on the amount of fluids available, whether from volatiles released from crystallizing apatite-iron oxide magma, the surrounding host rocks, marine sources, or meteoric waters. In particular, this metasomatic reworking of the fluorapatite may be assisted or reinforced by subsequent tectonothermal processes, such as, for example, the regional metamorphic overprinting at Grängesberg, or the ore body may have been affected by only moderate grades of regional metamorphism with little or no apparent deformation such as at Kiirunavaara or Pea Ridge. From the description and discussion above and the available fluid inclusion data, the types of fluids associated with the remobilization processes in such deposits are most likely Cl-dominated with a significant F component directly related to the amount of fluorapatite available in the system.

There is also experimental evidence that andesitic magmas may generate iron oxide-phosphate melts during the final stages of crystallization, due to strong melt polymerization (Lledo, 2005). Additional arguments, both physical and chemical, on how immiscible apatite-iron oxide

melts, couple with metasomatic processes, could form in conventional andesitic, dacitic, and rhyolitic magmas, typically associated with arc magmatism, are outlined in Chen et al. (2010) and Knipping et al. (2015). In contrast to magnetite and/or hematite, fluorapatite crystallizing out of these melts would act as a natural host for the (Y+REE) via either $Si^{4+} + (Y+REE)^{3+} = P^{5+} + Ca^{2+}$ or $Na^{+} + (Y+REE)^{3+} = 2Ca^{2+}$ (cf. Pan and Fleet, 2002). In metamorphic rocks, fluorapatite has also been shown to be a natural host for (Y+REE) at high temperature, as opposed to monazite at lower temperatures (cf. Hansen and Harlov, 2007). The observed high mobility of Fe, P, and REE in Cl-bearing fluids (e.g., Chou and Eugster, 1977; Antignano and Manning, 2008; Tropper et al., 2011, 2012; Lecumberri-Sanchez et al., 2015) would support the formation of monazite and xenotime associated with fluorapatite, as well as further interplay between the fluorapatite and the surrounding silicate mineral matrix, thus allowing for both the formation of independent monazite and xenotime grains as well as allanite. In the case of the Grängesberg deposit, an intrinsically volcanic/subvolcanic mode of formation was followed by a series of metasomatic pulses. This stage most likely started during the later phase of crystallization of the ore deposit and continued through the metamorphic and tectonic events experienced by the ores and host rocks during a prolonged geological evolution, a history in part recorded in the observed REE-bearing mineral assemblages in the Grängesberg district.

Acknowledgements

We thank Dieter Rhede for support with the electron microprobe at the GeoForschungsZentrum. The staff at the Geological Survey of Sweden (SGU) mineral office in Malå is thanked for their kind and enthusiastic help during drill core studies and sampling campaigns. This study is part of a larger project on the apatite-iron oxide deposits of the Grängesberg district, funded by the SGU.

References

Allen, R. L., Lundström, I., Ripa, M., Simeonov, A. and Christofferson, H. (1996) Facies analysis of a 1.9 Ga, continental margin, back-arc, felsic caldera province with diverse Zn-Pb-Ag-(Cu-Au) sulfide and Fe oxide deposits, Bergslagen region, Sweden. Economic Geology, 91, 979–1008.

Andersson, U. B. (1997) The late Svecofennian, high-grade contact and regional metamorphism in southwestern Bergslagen (central southern Sweden). Geological Survey of Sweden, research report 03-819/93. 29 pp.

Antignano, A. and Manning, C.E. (2008) Fluorapatite solubility in H_2O and H_2O-NaCl at 700 and 900 °C and 0.7 to 2.0 GPa. Chemical Geology, 251, 112–119.

Bonyadi, Z., Davidson, G.J., Mehrabi, B., Meffre, S. and Ghazban, F. (2011) Significance of fluorapatite REE depletion and monazite inclusions in the brecciated Se-Chahun iron oxide-fluorapatite deposit, Bafq district, Iran: Insights from paragenesis and geochemistry. Chemical Geology, 281, 253–269.

Boyce, J.W. and Hodges, K.V. (2005) U and Th zoning in Cerro de Mercado (Durango, Mexico) fluorapatite: Insights regarding the impact of recoil redistribution of radiogenic ^{4}He on (U-Th)/He thermochronology. Chemical Geology, 219, 261-274.

Broman, C., Nyström, J.O., Henriquez, F. and Elfman, M. (1999) Fluid inclusions in magnetite-fluorapatite ore from a cooling magmatic system at El Laco, Chile. Geologiska Föreningens i Stockholm Förhandlingar, 121, 253–267.

Budzyń, B., Harlov, D.E., Williams, M.L., Jercinovic, M.J. (2011) Experimental determination of stability relations between monazite, fluorapatite, allanite, and REE-epidote as a function of pressure, temperature, and fluid composition. American Mineralogist, 96, 1547–1567.

Chen, H., Clark, A.H. and Kyser, T.K. (2010) The Marcona magnetite deposit, Ica, south-central Peru: a product of hydrous, iron-oxide-rich melts? Economic Geology, 105, 1441-1456.

Chou, I.-M. and Eugster, H.P. (1977) Solubility of magnetite in supercritical chloride solutions. American Journal of Science, 277, 1296–1314.

Daliran, F. (1990) The magnetite–apatite deposit of Mishdovan, East-Central Iran. An alkali rhyolite hosted, “Kiruna-type” occurrence in the Infracambrian Bafg metallotect. Heidelberg Geowissenshaft Abhandlung, 37, 248.

Daliran, F. (2002) Kiruna-type iron oxide–apatite ores and “apatitites” of the Bafq District, Iran, with an emphasis on the REE geochemistry of their apatites. In Porter TM (Ed) Hydrothermal Iron Oxide Copper–Gold and related deposits, 2. PGC Publishing Australia, 303–320.

Daliran. F., Stosch, H.G., Williams, P., Jamali, H., and Dorri, M.B. (2010) Early Cambrian Iron Oxide-Apatite-REE (U) Deposits of the Bafq District, East-Central Iran (2010). in Coriveau L. and H. Mumin eds., Exploring for Iron Oxide Copper-Gold Deposits: Canada and Global Analogues. Geological Association of Canada, Short Course Notes 20, p.147–159.

Dong, P. (2005) Halogen-element (F, Cl and Br) behavior in aptites, scapolite and sodalite: An experimental investigation with field applications. Unpublished PhD thesis, University of Saskatchewan (free online access).

Finger, F., Broska, I., Roberts, M.P., and Schermaier, A. (1998) Replacement of primary monazite by apatite-allanite-epidote coronas in an amphibolite facies granite gneiss from the eastern Alps. American Mineralogist, 83, 248–258.

Förster, H. and Jafarzadeh, A. (1994) The Bafq mining district in central Iran – a highly mineralized infracambrian volcanic field. Economic Geology, 89, 1697–1721.

Förster, H.-J. (1998) The chemical composition of REE–Y–Th–U-rich accessory minerals from peraluminous granites of the Erzgebirge–Fichtelgebirge region, Germany. I. The monazite-(Ce) – brabantite solid solution series. American Mineralogist, 83, 259–272.

Frietsch, R. (1978) On the magmatic origin of iron ores of the Kiruna type. Economic Geology, 73, 478–485.

Frietsch, R. (1984) Petrochemistry of the iron ore-bearing metavolcanics in Norrbotten county, northern Sweden. Sveriges Geologiska Undersökning, Serie C, No. 802, 62 pp.

Frietsch, R., and Perdahl, J.-A. (1995) Rare earth elements in fluorapatite and magnetite in Kiruna-type iron ores and some other iron ore types. Ore Geology Reviews, 9, 489–510.

Geijer, P. (1910) Igneous rocks and iron ores of Kiirunavaara, Luossavaara and Tuolluvaara. Scientific and practical researches in Lapland arranged by Luossavaara-Kiirunavaara Aktiebolag. Ph.D. Thesis, Univ. Uppsala, Uppsala, Sweden.

Geijer, P. (1931) The iron ores of the Kiruna type: geographical distribution, geological characters, and origin. Sveriges Geologiska Undersökning, Serie C, No. 367, 39 pp.

Geijer, P. and Magnusson, N.H. (1944) De mellansvenska järnmalmernas geologi. Sveriges Geologiska Undersökning, Ca 35, 654 pp.

Geijer, P. (1967) Internal features of the apatite-bearing magnetite ores. Sveriges Geologiska Undersökning, Serie C, No. 624, 32 pp.

Goldoff, B., Webster, J.D., and Harlov, D.E. (2012) Characterization of fluor-chlorapatites by electron probe microanalysis with a focus on time-dependent intensity variation of halogens. American Mineralogist, 97, 1103–1115.

Goodenough, K.M., Schilling, J., Jonsson, E., Kalvig, P., Charles, N., Tuduri, J., Deady, E.A., Sadeghi, M., Schiellerup, H., Müller, A., Bertrand, G., Arvanitidis, N., Eliopoulos, D.G., Shaw, R.A, Thrane, K. and Keulen, N. (2016) Europe's rare earth element resource potential: an overview of metallogenetic provinces and their geodynamic setting. Ore Geology Reviews, 72, 838-856.

Gratz, R. and Heinrich, W. (1997) Monazite-xenotime thermobarometry: experimental calibration of the miscibility gap in the binary system $CePO_4$-YPO_4. American Mineralogist, 82, 772–780.

Hallberg, A. and Jonsson, E. (2006) Grängesberg – en järnmalms uppgång och fall. Geologiskt forum 13, 52, 17–21.

Hansen, E.C. and Harlov, D.E. (2007) Whole-rock, phosphate, and silicate compositional trends across an amphibolite- to granulite-facies transition, Tamil Nadu, India. Journal of Petrology, 48, 1641–1680.

Harlov, D.E., Andersson, U.B., Förster, H.J., Nyström, J.O., Dulski, P., and Broman, C. (2002a) Fluorapatite-monazite relations in the Kiirunavaara magnetite-fluorapatite ore, northern Sweden. Chemical Geology, 191, 47–72.

Harlov, D.E., Förster, H.J., and Nijland, T.G. (2002b) Fluid-induced nucleation of REE-phosphate minerals in fluorapatite: Nature and experiment. Part I. Chlorapatite. American Mineralogist, 87, 245–261.

Harlov, D.E. and Förster, H.J. (2003) Fluid-induced nucleation of (Y+REE)-phosphate minerals within fluorapatite: Nature and experiment. Part II. Fluorapatite. American Mineralogist, 88, 1209–1229.

Harlov, D.E., Wirth, R., and Förster, H.J. (2005) An experimental study of dissolution-reprecipitation in fluorapatite: fluid infiltration and the formation of monazite. Contributions to Mineralogy and Petrology, 150, 268–286.

Harlov, D.E., Meighan, C., Kerr, I., and Samson, I.M. (2016) Mineralogy, chemistry, and fluid-aided evolution of the Pea Ridge Fe-oxide-REE deposit, southeast Missouri, USA. Economic Geology (submitted).

Heinrich, W., Andrehs, G., and Franz, G. (1997) Monazite–xenotime miscibility gap thermometry: I. An empirical calibration. Journal of Metamorphic Geology, 15, 3–17.

Henriquez, F., Naslund, H.R., Nyström, J.O., Vivallo, W., Aguirre, R., Dobbs, F.M., and Lledo, H. (2003) New field evidence bearing on the origin of the El Laco magnetite deposit, northern Chile – a discussion. Economic Geology, 98, 1497–1500.

Hermansson, T., Stephens, M. B., Corfu, F., Andersson, J., and Page, L. (2007) Penetrative

ductile deformation and amphibolite-facies metamorphism prior to 1851 Ma in the western part of the Svecofennian orogen, Fennoscandian Shield. Precambrian Research, 153, 29–45.

Hitzman, M. W., Oreskes, N. & Einaudi, M. T. (1992) Geologic characteristics and tectonic setting of Proterozoic iron oxide (Cu-U-Au-REE) deposits. Precambrian Research, 58, 241-287.

Högdahl, K., Troll, V. R., Nilsson, K. P., and Jonsson, E. (2013) Structural evolution of the apatite-iron oxide deposit at Grängesberg, Bergslagen, Sweden. In: E. Jonsson et al. (eds.), Mineral deposit research for a high-tech world, Society for Geology Applied to Mineral Deposits, 1650–1653.

Islamovic, M., Åkerhammar, P., Norlin, L., Lundberg, C., and Baumgartner, A. (2015) Bergverksstatistik 2014 (Statistics of the Swedish mining industry 2014). Sveriges geologiska undersökning, periodiska publikationer 2015:1, 71 pp.

Jami, M., Dunlop, A.C., and Cohen, D.R. (2007) Fluid inclusion and stable isotope study of the Esfordi fluorapatite-magnetite deposit, Central Iran. Economic Geology, 102, 1111–1125.

Janots, E., Brunet, F., Goffé, B., Poinssot, C., Burchard, M., and Cemic, L. (2007) Thermochemistry of monazite-(La) and dissakisite-(La): implications for monazite and allanite stability in metapelites. Contributions to Mineralogy and Petrology, 154, 1–14.

Janots, E., Engi, M., Berger, A., Allaz, J., Schwarz, J.O., and Spandler, C. (2008) Prograde metamorphic sequence of REE minerals in pelitic rocks of the Central Alps: implications for allanite–monazite–xenotime phase relations from 250 to 610 °C. Journal of Metamorphic Geology, 26, 509–526.

Jarosewich, E., Nelen, J.A., and Norberg, J.A. (1980) Reference samples for electron microprobe analysis. Geostandards Newsletter, 4, 43–47.

Jarosewich, E. and Boatner, L.A. (1991) Rare-earth element reference samples for electron microprobe analysis. Geostandards Newsletter, 15, 397–399.

Johansson, H. (1910) Die eisenerzführende Formation in der Gegend von Grängesberg. Geologiska Föreningens i Stockholm Förhandlingar, 32, 239–410.

Jonsson, E., Nilsson, K.P., Hallberg, A, and Högdahl, K. (2010a) The Palaeoproterozoic fluorapatite-iron oxide deposits of the Grängesberg area: Kiruna-type deposits in central Sweden. In: Nakrem H A, Harstad AO, Haukdal G (eds.) NGF abstracts and proceedings vol. 1: 88–89.

Jonsson, E., Persson Nilsson, K., Högdahl, K., Troll, V. R., and Hallberg, A. (2010b) REE distribution and mineralogy in a Palaeoproterozoic apatite-iron oxide deposit: Grängesberg, Bergslagen, Sweden. Acta Mineralogica-Petrographica abstract series 6, 234.

Jonsson, E., Persson Nilsson, K., Hallberg, A., Högdahl, K., Troll, V. R., Weis, F., and Harris, C. (2011) Oxygen isotopes and geochemistry of Palaeoproterozoic Kiruna-type deposits in the Bergslagen province, Sweden. 11th Biennial SGA meeting, Antofagasta, Chile. Abstract volume, 494–496.

Jonsson, E., Troll, V. R., Högdahl, K., Harris, C., Weis, F., Nilsson, K. P. and Skelton, A. (2013) Magmatic origin of giant central Swedish ”Kiruna-type” apatite-iron oxide ores. Scientific Reports 3: 1644, 1–8.

Kerr, I.D. (1998) Mineralogy, chemistry, and hydrothermal evolution of the Pea Ridge Fe-oxide-REE deposit, Missouri, USA. Masters Thesis, University of Windsor, Windsor, Ontario, Canada, 113 pp.

Kisvarsanyi, E.B., and Kisvarsanyi, G., (1989) Alkaline granite ring complexes and metallogeny in the middle Proterozoic St. Francois Terrane, southeastern Missouri, USA. In Mid-Proterozoic Laurentia-Baltica (C.F. Gower, T. River, and B. Ryan, eds.) Geological Association of Canada, Special Paper 38, p. 433–446.

Knipping, J.L., Bilenker, L.D., Simon, A.C., Reich, M., Barra, F., Deditius, A.P., Lundstrom, C., Bindeman, I., and Munizaga, R., (2015) Giant Kiruna-type deposits form by efficient flotation of magmatic magnetite suspensions. Geology, 43, 591-594.

Leake, B.E., Woolley, A.R., Arps, C.E.S., Birch, W.D., Gilbert, M.C., Grice, J.D., Hawthorne, F.C., Kato, A., Kisch, H.J., Krivovichev, V.G., Linthout, K., Laird, J., Mandarino, J.A., Maresch, W.V., Nickel, E.H., Rock, N.M.S., Schumacher, J.C., Smith, D.C., Stephenson, N.C.N., Ungaretti, L., Whittaker, E.J.W., and Youzhi, G. (1997) Nomenclature of amphiboles: Report of the subcommittee on amphiboles of the international mineralogical association commission on new minerals and mineral names. Canadian Mineralogist, 35, 219–246.

Lecumberri-Sanchez, P., Steele-MacInnis, M., and Bodnar, R.J. (2015) Synthetic fluid inclusions XIX. Experimental determination of the vapor-saturated liquidus of the system H_2O-NaCl-$FeCl_2$. Geochimica et Cosmochimica Acta, 148, 34–49.

Lledó, L.H., (2005) Experimental studies on the origin of iron deposits and mineralization of Sierra La Bandera, Chile: Unpublished Ph.D. thesis, Binghamton, New York, State University of New York, 200 p.

Looström, R. (1929) Likheter mellan Lapplands- och Grängesbergsmalmerna: Geologiska Föreningens i Stockholm Förhandlingar, 51, 303-308.

Looström, R. (1939) Lönnfallet. Southernmost part of the Export field at Grängesberg. Sveriges Geologiska Undersökning Serie C, 428, 30 pp.

Lupulescu, M.V. and Pyle, J.M. (2005) The Fe-P-REE deposit at Mineville, Essex Co., NY;

manifestations of Precambrian and Mesozoic fluid infiltration events. Anonymous. Abstracts with Programs – Geological Society of America 37, 4.

Lupulescu, M.V. and Pyle, J.M. (2008) Mining history, mineralogy and origin of the gneiss (granite)-hosted Fe-P-REE and Fe oxide and gabbro-hosted Ti-Fe deposits from the Mineville-Port Henry region, Essex County, NY. Guidebook – New York State Geological Association, Meeting, 80, pp. 117–129.

Magnusson, N.H. (1938) Neue Untersuchungen innerhalb des Grängesberg-Feldes. Sveriges Geologiska Undersökning Serie C, 418, 44 pp.

Magnusson, N.H. (1970) The origin of the iron ores in central Sweden and the history of their alterations, vols. I- II. Sveriges Geologiska Undersökning Serie C, 643, 127+364 pp.

Marikos, M.A., Nuelle, L.M., and Seeger, C.M. (1989) Geology of the Pea Ridge Mine. In Olympic dam-type " deposits and geology of middle Proterozoic rocks in the St. Francois Mountains Terrane, Missouri, Society of Economic Geologists (eds. Marikos, M.A., Nuelle, L.M., Seeger, and Cheryl M.), pp.

McKeown, F.A. and Klemic, H. (1956) Rare-earth-bearing fluorapatite at Mineville, Essex County, New York. U.S. Geological Survey Bulletin (1956), pp. 9–23.

Mücke, A. and Younessi, R. (1994) Magnetite-fluorapatite deposits (Kiruna-type) along the Sanandaj-Sirjan zone and in the Bafq area, Iran, associated with ultramafic and calcalkaline rocks and carbonatites. Mineralogy and Petrology, 50, 219–244.

Naranjo, J.A., Henriquez, F., and Nyström, J.O. (2010) Subvolcanic contact metasomatism at El Laco volcanic complex, central Andes. Andean Geology, 37, 110–120.

Naslund, H.R., Aguirre, R., Dobbs, F.M., Henriquez, F., and Nyström, J.O. (2000) The origin, emplacement, and eruption of ore magmas. IX Congreso Geologico Chileno, Actas, 2, 135–139.

Naslund, H.R., Henriquez, F., Nyström, J.O., Vivallo, W., and Dobbs, F.M. (2002) Magmatic iron ores and associated mineralization: examples from the Chilean High Andes and Coastal Cordillera. In Porter, T.M., ed., Hydrothermal Iron Oxide Copper-Gold & Related Deposits: A Global Perspective, volume 2, PGC Publishing, Adelaide, pp. 207–226.

Nyström, J.O. and Henriquez, F. (1989) Dendritic magnetite and miniature diapirs-like concentrations of apatite: two magmatic features of the Kiirunavaara iron ore. Geologiska Föreningens i Stockholm Förhandlingar, 111, 53–64.

Nyström, J.O. and Henriquez, F. (1994) Magmatic features of iron ores of the Kiruna type in Chile and Sweden: ore textures and magnetite geochemistry. Economic Geology, 89, 820–839.

Nyström, J.O., Billström, K., Henriquez, F., Fallick, A.E., and Naslund, H.R. (2008) Oxygen

isotope composition of magnetite in iron ores of the Kiruna type in Chile and Sweden. Geologiska Föreningens i Stockholm Förhandlingar, 130, 177–188.

Persson, K.P., Högdahl, K., Jonsson, E., Troll, V.R., Weis, F., Persson, L., Majka, J., and Skelton, A. (2013) The Grängesberg apatite-iron oxide deposit. Sveriges Geologiska Undersökning report, projects 35189 and 60-1629/2008. 45 pp.

Pouchou, J.L. and Pichoir, F. (1985) "PAP" (φ-ρ-Z) procedure for improved quantitative microanalysis. In: Armstrong, J.T. (ed.) Microbeam Analysis. San Francisco: San Francisco Press, pp. 104–106.

Pan, Y. and Dong, P. (1999) The Lower Changjiang (Yangzi/Yangtze River) metallogenic belt, east central China: intrusion- and wall rock-hosted Cu–Fe–Au, Mo, Zn, Pb, Ag deposits. Ore Geology Reviews, 15, 177-242.

Pan, Y., Fleet, M.E., and Macrae, N.D. (1993) Oriented monazite inclusions in apatite porphyroblasts from the Hemlo gold deposit, Ontario, Canada. Mineralogical Magazine, 57, 697–707.

Pan, Y. and Fleet M.E. (2002) Composition of the fluorapatite-group minerals: Substitution mechanisms and controlling factors. In M. J. Kohn, J. Rakovan, and J. M. Hughes., Phosphates: Geochemical, Geobiological and Materials Importance, 48, 13–49. Reviews in Mineralogy, Mineralogical Society of America, Washington, D.C.

Putnis, A. (2009) Mineral replacement reactions. Thermodynamics and kinetics of water-rock interaction, Reviews in Mineralogy and Geochemistry, (in Oelkers, E.H. and Schott, J. editors) vol. 70, pp. 87–124.

Putnis, A. and Austrheim, H. (2012) Mechanisms of metasomatism and metamorphism on the local mineral scale: the role of dissolution-reprecipitation during mineral re-equilibration. in Metasomatism and the Chemical Transformation of Rock: The Role of Fluids in Terrestrial and Extraterrestrial Processes (D. Harlov and H. Austrheim, eds.), Spinger, Heidelberg, p. 141–170.

Pyle, J.M., Spear, F.S., and Wark, D.A. (2002) Electron Microprobe Analyses of REE in Fluorapatite, Monazite and Xenotime: Protocols and Pitfalls. In Kohn, J.M., Rakovan, J. & Hughes, J.M. (eds) Phosphates: Geochemical, Geobiological and Materials Importance. Reviews in Mineralogy and Geochemistry, 48, 337–362.

Sidder, G.B., Day, W.C., Nuelle, L.M., Seeger, C.M., and Kisvarsanyi, E.B. (1993) Mineralogic and fluid-inclusion studies of the Pea Ridge iron-rare-earth-element deposit, Southeast Missouri. U.S. Geological Survey Bulletin, 1993, 205–216.

Stephens, M.B., Ripa, M., Lundström, I., Persson, L., Bergman, T., Ahl, M., Wahlgren, C.-H.,

Persson, P.-O., and Wickström, L. (2009) Synthesis of the bedrock geology in the Bergslagen region, Fennoscandian Shield, south-central Sweden. Sveriges Geologiska Undersökning Ba 58, 1-259.

Stormer, J.C., Jr., Pierson, M.J., and Tacker, R.C. (1993) Variation of F and Cl X-ray intensity due to anisotropic diffusion of fluorapatite during electron microprobe analyses. American Mineralogist, 78, 641–648.

Stosch, H.-G., Romer, R.L., Daliran, F., and Rhede, D. (2011) Uranium-lead ages of apatite from iron oxide ores of the Bafq District. East-Central Iran. Mineralium Deposita, 46, 9–21.

Spear, F.S. (2010) Monazite–allanite phase relations in metapelites. Chemical Geology, 279, 55–62.

Taghipour, S., Kananian, A., Harlov, D., and Oberhänsli, R. (2015) Kiruna-type iron oxide-apatite deposits, Bafq district, central Iran: Fluid-aided genesis of fluorapatite-monazite-xenotime assemblages. The Canadian Mineralogist, 53, 1–17.

Tegengren, F. (1924) Sveriges ädlare malmer och bergverk. Sveriges Geologiska Undersökning Ca 17, 406 pp.

Torab, F.M. and Lehmann, B. (2007) Magnetite-fluorapatite deposits of the Bafq district, Central Iran: fluorapatite geochemistry and monazite geochronology. Mineralogical Magazine, 71, 347–363.

Treloar, P. J. and Colley, H. (1996) Variations in F and Cl contents in apatites from magnetite-apatite ores in northern Chile, and their ore-genetic implications. Mineralogical Magazin,e 60, 285–301.

Tropper, P., Manning, C.E., and Harlov, D.E. (2011) Solubility of $CePO_4$ monazite and YPO_4 xenotime in H_2O and H_2O-NaCl at 800 °C and 1 GPa: Implications for REE and Y transport during high-grade metamorphism. Chemical Geology, 282, 58–66.

Tropper, P., Manning, C.E., and Harlov, D.E. (2013) Experimental determination of $CePO_4$ and YPO_4 solubilities in H_2O-NaF at 800°C and 1 GPa: implications for rare earth element transport in high-grade metamorphic fluids. GeoFluids, 13, 372–380.

Weis, F., Troll, V.R., Jonsson, E., Högdahl, K., Barker, A., Harris, C., Millet, M.-A., and Nilsson, K.P. (2013) Iron and oxygen isotope characteristics of apatite-iron-oxide ores from central Sweden. In: E. Jonsson et al. (eds.), Mineral deposit research for a high-tech world, Society for Geology Applied to Mineral Deposits, 1675-1678.

Williams, P.J., Barton, M.D., Johnson, D.A., Fontboté, L., De Haller, A., Mark, G., Oliver, N.H.S., and Marschik, R. (2005) Iron oxide copper-gold deposits: geology, space-time distribution, and possible modes of origin. Economic Geology 100th anniversary volume, 371-405.

Whitten, C.W. and Yancey R.J. (1990) Characterization of the Rare-Earth Mineralogy at the Pea Ridge Deposit, Missouri. Report of Investigations 9331. Unite States Department of the Interior, Brureau of Mines, 9pp.

Young, E.J., Myers, A.T., Munson, E.L., and Conklin, N.M. (1969) Mineralogy and chemistry of fluorapatite from Cerro de Mercado, Durango, Mexico. USGS Professional Paper 650-D, D84-D93.

Figures

Figure 1: (**a)** Geological map of the Grängesberg District, Bergslagen, south central Sweden. Modified after Geijer and Magnusson, 1944. (**b**) Geological profile, as outlined in 1a, showing the dip of the ore zone, and relations between the ore and its associated rocks. Based on datasets from the Geological Survey of Sweden (SGU), and A. Hallberg, SGU.

Figure 2: High contrast BSE images of typical oxide textures in the Grängesberg magnetite-hematite-fluorapatite ores. (**a**) Coarse, subhedral magnetite crystals embedded in a finer-grained hematite-silicate groundmass. (**b**) Granoblastic magnetite with elongated, banding-parallel fluorapatite aggregates. (**c**) Granoblastic magnetite-hematite ore. (**d**) Distinctly foliated hematite-magnetite ore with bands of silicates. Bt = biotite, FAp = fluorapatite, Hm = hematite, Mt = magnetite, Qtz = quartz.

Figure 3: High contrast BSE images of REE-zoned fluorapatite in the magnetite-hematite-fluorapatite ores (Type 1 assemblages). (**a-b**) Granoblastic magnetite-fluorapatite ore. Note that lighter areas in fluorapatite are relatively enriched in Y+REE compared to the darker ones. (**c**) Zoned fluorapatite with abundant, small inclusions of monazite in the (Y+REE)-depleted core region. Note crystallographically controlled orientation of monazite inclusions. (**d**) Zoned and unzoned fluorapatite crystals. The relatively bigger grain of monazite in the unzoned fluorapatite crystallized as an effect of the Ostwald ripening process. Minor allanite can be seen as a fracture-filling in the lower right part of the image. FAp = fluorapatite, Mnz = monazite-(Ce), Mt = magnetite.

Figure 4: High contrast BSE images of monazite inclusions in fluorapatite. (**a**) Monazite inclusions in unzoned fluorapatite in the altered host rocks (sköl rocks; Type 3 assemblages) (**b-d**) Abundant monazite and xenotime inclusions in fluorapatite breccias (Type 2 assemblages). Here allanite is seen filling in cracks and cavities in the fluorapatite. The allanite typically occurs in or near fluorapatite that has few or no monazite or xenotime inclusions. Aln = allanite-(Ce), Bt = biotite, Mt = magnetite, Plg = plagioclase, Qtz = quartz.

Figure 5: High contrast BSE images of various allanite textures associated with fluorapatite and as independent grains. (**a**) Allanite filling in cracks and voids within an isolated fluorapatite grain in the altered, metavolcanic host rock (Type 3 assemblage). (**b**) shows an enlargement of the box in

(**a**). (**c**) Allanite is seen growing along fluorapatite grain boundaries in a sample from the apatite-iron oxide ores (Type 1 assemblage). (**d**) Isolated allanite grains in the altered host rock groundmass (sköl; Type 3 assemblage), in which the allanite is associated, and in part intergrown with magnetite.

Figure 6: Plot showing that the dominant coupled substitution for (Y+REE) in fluorapatite is Si^{4+} + $(Y+REE)^{3+} = P^{5+} + Ca^{2+}$, as evidenced by the linear correlation between Si and (Y+REE).

Tables

Table 1: Mineralogy of the Grängesberg ore district.

Table 2: Mean fluorapatite compositions (wt%).

Table 3: Representative monazite and xenotime compositions (wt%).

Table 4: Representative analyses of allanite (wt%).

Supplementary material

Appendix A: EMP analyses of fluorapatite.

Appendix B: EMP analyses of monazite and xenotime

Appendix C: EMP analyses of allanite.

This is a preprint, the final version is subject to change, of the American Mineralogist (MSA)
Cite as Authors (Year) Title. American Mineralogist, in press.
(DOI will not work until issue is live.) DOI: http://dx.doi.org/10.2138/am-2016-5655

Table 1: Mineralogy of the Grängesberg ore district

	Sample	Locality	Lithological Type	Description	Location	FAp	Mnz	Xn	Aln	Mt	Hm	Ilm	Zrn
1	KES090053	Grängesberg	Type 3	volcanic "grey leptite"segregation	borehole 717	+			+	+			+
2	KES090065	Grängesberg	Type 3	altered volcanic rock with Mt-FAp veins	borehole 717	+	+	+		+		+	
3	KES090070	Grängesberg	Type 1	massive Mt ore	borehole 717	+	+			+			
4	KES090073	Grängesberg	Type 1	massive Mt ore	borehole 717	+	+			+			
5	KES090074	Grängesberg	Type 3	schistose volcanic rock	borehole 717	+			+	+			+
6	KES090076	Grängesberg	Type 1	massive Hm ore	borehole 717	+	+				+		
7	KES090077	Grängesberg	Type 1	Mt-Hm ore	borehole 717	+				+	+		
8	KES090078	Grängesberg	Type 1	Ap-veined Hm ore	borehole 717	+	+		+		+		
9	KES090079	Grängesberg	Type 1	Hm-Mt ore	borehole 717	+	+	+	+	+	+		
10	KES090081	Grängesberg	Type 3	alteration zone, contact with Hm-Mt ore	borehole 717	+	+		+	+	+		
11	KES090083	Grängesberg	Type 3	Mt-banded volcanic rock	borehole 717	+			+	+			+
12	KES090084	Grängesberg	Type 3	banded impregnation of Mt+Hm in volcanics	borehole 717	+			+	+	+		
13	KES090088A	Grängesberg	Type 3	finely banded Mt-calc-silicate	borehole 717	+			+			+	
14	LAL042047	Grängesberg	Type 1	Mt-Hm ore	borehole 690	+			+	+	+		
15	KHO090003	Grängesberg	Type 3	Mt-bearing volcanite 1 km W from the ore	outcrop	+	+			+			
16	KHO090005	Grängesberg	Type 2	volcanic breccia	outcrop	+	+						
17	KHO090010	Grängesberg	Type 2	apatite breccia	outcrop	+	+	+	+		+		
18	KHO090011	Grängesberg	Type 2	volcanic breccia	outcrop	+	+		+	+	?		
19	KHO090128	Grängesberg	Type 1	Hm-Mt layered ore	outcrop	+	+		+	+	+		
20	KES091011A	Gudmundsberget	Type 1	banded Hm-Mt ore	outcrop	+			+	+	+		
21	KES09016B	Fallgruvan	Type 1	Mt ore	outcrop	+	+			+		+	

This is a preprint, the final version is subject to change, of the American Mineralogist (MSA)
Cite as Authors (Year) Title. American Mineralogist, in press.
(DOI will not work until issue is live.) DOI: http://dx.doi.org/10.2138/am-2016-5655

Table 2: Mean fluorapatite compositions (wt%)

Sample	Locality	Description	# pts	P_2O_5	SiO_2	SO_3	Y_2O_3	La_2O_3	Ce_2O_3	Pr_2O_3	Nd_2O_3	CaO	MnO
KES090053	Grängesberg	volcanic "grey leptite"	25	41.79	0.29	0.01	0.13	0.07	0.16	0.06	0.11	55.08	0.04
		segregation		*0.81*	*0.26*	*0.01*	*0.10*	*0.06*	*0.11*	*0.06*	*0.09*	*0.54*	*0.03*
KES090065	Grängesberg	altered volcanic rock with Mt-Fap veins	35	41.94	0.12	0.04	0.23	0.03	0.07	0.07	0.12	55.01	0.03
				0.48	*0.04*	*0.02*	*0.03*	*0.03*	*0.05*	*0.05*	*0.07*	*0.26*	*0.02*
KES090070	Grängesberg	massive Mt ore	23	41.55	0.09	0.03	0.17	0.02	0.07	0.04	0.08	54.78	0.02
				0.43	*0.07*	*0.02*	*0.04*	*0.03*	*0.05*	*0.05*	*0.06*	*0.23*	*0.02*
KES090073	Grängesberg	massive Mt ore	19	39.09	0.14	0.03	0.11	0.07	0.18	0.07	0.10	55.13	0.01
		dark zones in Fap		*1.39*	*0.08*	*0.02*	*0.05*	*0.06*	*0.07*	*0.08*	*0.09*	*0.36*	*0.02*
KES090073	Grängesberg	massive Mt ore	15	37.57	0.74	0.11	0.43	0.18	0.60	0.13	0.39	53.99	0.02
		light zones in Fap		*1.22*	*0.22*	*0.04*	*0.12*	*0.09*	*0.22*	*0.09*	*0.11*	*0.49*	*0.03*
KES090074	Grängesberg	schistose volcanic rock	25	41.71	0.16	0.03	0.11	0.02	0.01	0.02	0.03	55.83	0.01
				0.51	*0.23*	*0.02*	*0.02*	*0.03*	*0.02*	*0.03*	*0.04*	*0.44*	*0.02*
KES090076	Grängesberg	massive Hm ore	22	41.36	0.19	0.04	0.16	0.03	0.10	0.06	0.09	54.62	0.02
				0.44	*0.14*	*0.03*	*0.05*	*0.04*	*0.07*	*0.07*	*0.06*	*0.38*	*0.02*
KES090077	Grängesberg	Mt-Hm ore	22	41.63	0.17	0.04	0.14	0.02	0.09	0.04	0.10	54.81	0.02
				0.73	*0.50*	*0.02*	*0.02*	*0.03*	*0.07*	*0.03*	*0.07*	*0.45*	*0.02*
KES090078	Grängesberg	Ap-veined Hm ore	20	41.38	0.09	0.04	0.19	0.04	0.08	0.03	0.11	54.91	0.01
				0.31	*0.03*	*0.02*	*0.02*	*0.04*	*0.07*	*0.05*	*0.08*	*0.40*	*0.02*
KES090079	Grängesberg	He-Mt ore	24	41.50	0.23	0.06	0.32	0.04	0.12	0.07	0.12	54.83	0.07
				0.57	*0.18*	*0.04*	*0.18*	*0.04*	*0.10*	*0.07*	*0.09*	*0.48*	*0.04*
KES090081	Grängesberg	alteration zone, contact to He-Mt ore	28	41.44	0.14	0.04	0.18	0.05	0.09	0.03	0.09	54.71	0.05
				0.57	*0.10*	*0.03*	*0.11*	*0.06*	*0.08*	*0.06*	*0.07*	*0.65*	*0.04*
KES090083	Grängesberg	Mt-banded volcanic rock	24	41.19	0.16	0.03	0.24	0.01	0.03	0.02	0.04	54.87	0.02
				0.73	*0.31*	*0.03*	*0.38*	*0.02*	*0.04*	*0.04*	*0.04*	*0.60*	*0.02*
KES090084	Grängesberg	banded impregnation of Mt+He in volc.	25	41.21	0.11	0.03	0.23	0.02	0.04	0.04	0.04	54.64	0.02
				0.59	*0.16*	*0.02*	*0.22*	*0.03*	*0.05*	*0.05*	*0.05*	*0.43*	*0.02*

KES090088A	Grängesberg	finely banded Mt-calc-silicate	29	42.11	0.11	0.03	0.10	0.03	0.04	0.03	0.06	55.58	0.04
				0.50	*0.05*	*0.03*	*0.04*	*0.04*	*0.06*	*0.05*	*0.07*	*0.26*	*0.03*
LAL042047	Grängesberg	Mt-He ore	20	41.853	0.17	0.03	0.22	0.03	0.02	0.03	0.03	55.62	0.02
				0.4146	*0.09*	*0.02*	*0.10*	*0.03*	*0.02*	*0.03*	*0.04*	*0.28*	*0.02*
KHO090010	Grängesberg	apatite breccia	25	41.91	0.26	0.01	0.21	0.03	0.06	0.02	0.06	55.01	0.04
				0.63	*0.40*	*0.01*	*0.05*	*0.04*	*0.06*	*0.03*	*0.06*	*0.56*	*0.02*
KHO090011	Grängesberg	volcanic breccia	25	41.88	0.18	0.01	0.25	0.02	0.02	0.03	0.04	55.49	0.04
				0.43	*0.15*	*0.01*	*0.20*	*0.03*	*0.02*	*0.03*	*0.05*	*0.37*	*0.02*
KHO090128	Grängesberg	Hm-Mt layered ore	25	41.84	0.11	0.04	0.11	0.02	0.03	0.02	0.05	55.70	0.02
				0.46	*0.16*	*0.01*	*0.03*	*0.03*	*0.05*	*0.04*	*0.05*	*0.44*	*0.02*
KES091011A	Gudmundsberget	banded Hm-Mt ore	25	40.84	0.26	0.05	0.26	0.04	0.12	0.04	0.12	54.83	0.02
				0.44	*0.17*	*0.02*	*0.17*	*0.04*	*0.10*	*0.04*	*0.08*	*0.46*	*0.02*
KES09016B	Fallgruvan	Mt ore	25	41.46	0.09	0.03	0.14	0.02	0.06	0.02	0.07	54.70	0.03
				0.37	*0.02*	*0.01*	*0.05*	*0.02*	*0.05*	*0.05*	*0.05*	*0.28*	*0.02*

1 σ - standard deviation in italics; a = total Fe as FeO; b = calculated assuming the (F,Cl,OH) site is filled; blank - with the exception of H_2O, measured for but not detecte

FeO	Na_2O	SrO	F	Cl	H_2O^b	sum	O=(F+Cl)	total	$(Y+LREE)_2O_3$
0.13	0.02	0.00	4.17	0.01	0.03	102.08	1.76	100.32	0.52
0.18	*0.02*	*0.00*	*0.37*	*0.01*	*0.01*				
0.03	0.13	0.00	4.34	0.01		102.17	1.83	100.34	0.52
0.03	*0.04*	*0.00*	*0.21*	*0.01*					
0.14	0.10	0.01	3.21	0.11	0.18	100.60	1.38	99.22	0.37
0.16	*0.03*	*0.03*	*0.18*	*0.03*	*0.07*				
0.16	0.07	0.00	4.61	0.01		99.79	1.94	97.84	0.53
0.22	*0.03*	*0.00*	*0.40*	*0.01*					
0.12	0.09	0.00	4.30	0.02		98.69	1.82	96.88	1.73
0.26	*0.05*	*0.00*	*0.30*	*0.01*					
0.07	0.02	0.03	4.14	0.01		102.20	1.74	100.46	0.19
0.13	*0.02*	*0.02*	*0.16*	*0.01*					
0.35	0.06	0.00	4.03	0.02		101.14	1.70	99.44	0.44
0.35	*0.02*	*0.00*	*0.31*	*0.01*					
0.24	0.10	0.00	4.08	0.02	0.05	101.55	1.72	99.82	0.40
0.29	*0.04*	*0.00*	*0.30*	*0.02*	*0.06*				
0.02	0.11	0.00	4.09	0.01		101.10	1.72	99.37	0.44
0.02	*0.02*	*0.00*	*0.19*	*0.01*					
0.17	0.10	0.00	4.25	0.01	0.02	101.90	1.79	100.11	0.67
0.22	*0.04*	*0.00*	*0.29*	*0.01*	*0.01*				
0.18	0.09	0.00	4.63	0.01		101.71	1.95	99.76	0.43
0.15	*0.06*	*0.00*	*0.28*	*0.01*					
0.50	0.05	0.00	4.57	0.01	0.02	101.76	1.93	99.84	0.34
0.36	*0.03*	*0.00*	*0.45*	*0.01*	*0.01*				
0.30	0.06	0.00	4.35	0.01		101.08	1.83	99.25	0.37
0.15	*0.03*	*0.00*	*0.18*	*0.01*					

This is a preprint, the final version is subject to change, of the American Mineralogist (MSA)
Cite as Authors (Year) Title. American Mineralogist, in press.
(DOI will not work until issue is live.) DOI: http://dx.doi.org/10.2138/am-2016-5655

0.20	0.03	0.00	4.30	0.03	0.04	102.75	1.82	100.93	0.27
0.17	0.03	0.00	0.47	0.02	0.02				
0.24	0.03	0.03	4.48	0.00		102.80	1.89	100.92	0.32
0.12	*0.02*	*0.02*	*0.12*	*0.01*					
0.12	0.04	0.00	3.62	0.17	0.11	101.68	1.56	100.11	0.38
0.30	*0.03*	*0.00*	*0.30*	*0.08*	*0.06*				
0.06	0.04	0.03	3.69	0.12		101.88	1.58	100.30	0.36
0.03	*0.03*	*0.02*	*0.28*	*0.08*					
0.21	0.06	0.04	4.11	0.02		102.37	1.73	100.64	0.24
0.17	*0.03*	*0.02*	*0.08*	*0.01*					
0.35	0.07	0.04	4.82	0.00		101.87	2.03	99.84	0.58
0.21	*0.03*	*0.02*	*0.23*	*0.00*					
0.10	0.06	0.04	4.63	0.05		101.49	1.96	99.53	0.31
0.11	*0.03*	*0.02*	*0.29*	*0.01*					

d.

Table 3: Representative monazite and xenotime compositions (wt%)

Sample	Locality	Description	Comment	P_2O_5	SiO_2	ThO_2	UO_2	Al_2O_3	Y_2O_3	La_2O_3	Ce_2O_3	Pr_2O_3	Nd_2O_3	Sm_2O_3	Eu_2O_3	Gd_2O_3	Tb_2O_3	Dy_2O_3	Ho_2O_3	Er_2O_3	Yb_2O_3	Lu_2O_3	CaO	PbO	FeO	SrO	MgO	sum
KES090065	Grängesberg	altered volcanic rock with Mt-FAp veins	tiny grain in FAp	30.32	0.38	0.47			0.78	16.47	34.25	3.20	11.41	1.19		0.85		0.15		0.07			0.99	0.07				100.59
KES090065	Grängesberg	altered volcanic rock with Mt-FAp veins	big grain in FAp	30.35	0.28	0.42			0.91	15.64	34.36	3.30	12.19	1.35	0.05	0.82		0.19		0.08			0.21	0.08				100.23
KES090070	Grängesberg	massive Mt ore	in FAp	29.29	0.29	0.56			0.78	18.94	33.39	2.87	10.28	1.23		0.80		0.06					0.44	0.09				99.01
KES090073	Grängesberg	massive Mt ore	tiny grain in FAp	30.51	0.30				0.23	18.78	34.61	3.17	8.99	0.68	na	0.18	na	0.09		na	0.09		2.38			na	na	100.01
KES090076	Grängesberg	massive Hm ore	outside FAp	29.41	0.34	0.16			0.32	19.06	34.97	2.94	9.93	1.05		0.46	0.06	0.00			0.09		0.69		0.23			99.71
KES090077	Grängesberg	Mt-Hm ore	in Fe-oxide	29.63	0.30	0.84			0.64	18.44	32.52	2.76	9.73	0.89		0.71		0.09					0.26	0.07	1.55			98.431
KES090078	Grängesberg	FAp-veined Hm ore	in FAp	29.25	0.27	0.34			0.41	21.35	35.11	2.79	8.22	0.68	0.12	0.39		0.02	0.05	0.06			0.28	0.07				99.42
KES090081	Grängesberg	alteration zone contact to Hm-Mt ore	tiny grain in FAp	28.46	0.76	0.32			0.45	19.64	33.37	2.95	10.15	1.19	0.05	0.68	0.08	0.07	0.06				0.41					98.64
KES090081	Grängesberg	alteration zone contact to Hm-Mt ore	big grain in FAp	29.86	0.30	0.06			0.63	17.92	32.93	3.08	11.34	1.22	0.29	0.93		0.12				0.06	0.32					99.07
KHO090010	Grängesberg	apatite breccia	tiny grain in FAp	29.73	0.37	0.95			0.69	17.66	33.79	3.09	11.13	1.03		0.59	0.15	0.07					1.77	0.09				101.11
KHO090010	Grängesberg	apatite breccia	big grain in FAp	29.53	0.68	0.15			0.44	18.64	34.11	3.08	10.50	1.06	0.05	0.67	0.08	0.05		0.07	0.07		1.62					100.79
KHO090010	Grängesberg	apatite breccia	xenotime in FAp	35.34	0.12		0.12		44.36	0.00	0.00	0.00	0.22	0.27	1.26	4.62	0.69	4.72	1.16	3.68	2.96	0.24	0.51					100.29
KHO090128	Grängesberg	Hm-Mt layered ore	in Fe-oxide	29.83	0.14				0.54	24.79	33.04	2.19	5.94	0.41	0.19	0.37	0.08	0.15	0.10	0.18			0.23			0.06		98.227
KES09016B	Fallgruvan	Mt ore	in FAp	29.58	0.48	2.04			1.40	15.38	30.97	2.94	10.79	1.29	0.31	1.00	0.05	0.19					0.45	0.19				97.047
KES09016B	Fallgruvan	Mt ore	in Fe-oxide	29.27	0.47	2.10			1.64	15.28	30.34	3.04	10.89	1.45	0.27	1.10	0.07	0.21	0.05	0.11	0.07		0.64	0.16	0.18			97.34

blank - measured for, but not detected, na - not analysed

This is a preprint, the final version is subject to change, of the American Mineralogist (MSA)
Cite as Authors (Year) Title. American Mineralogist, in press.
(DOI will not work until issue is live.) DOI: http://dx.doi.org/10.2138/am-2016-5655

Table 4: Representative analyses of allanite (wt%)

Sample	Locality	Description	Comment	P_2O_5	SiO_2	ThO_2	UO_2	Al_2O_3	Y_2O_3	La_2O_3	Ce_2O_3	Pr_2O_3	Nd_2O_3	Sm_2O_3	Eu_2O_3	Gd_2O_3	Tb_2O_3	Dy_2O_3	Ho_2O_3	Er_2O_3	Yb_2O_3	Lu_2O_3	MgO	FeO	CaO	SrO	PbO	sum
KES 090053	Grängesberg	volcanic "grey leptite" segregation	matrix		32.36	0.45	0.05	16.42	0.00	6.33	9.48	0.63	1.97	0.11		0.02				0.23			0.28	12.85	11.84			93.03
KES090074	Grängesberg	schistose volcanic rock	in FAp		33.25			16.81	0.23	4.16	6.84	0.71	2.39	0.28		0.19			0.10				1.45	14.01	15.62			96.02
KES090077	Grängesberg	Mt-Hm ore	in Fe-oxide		29.76			10.67		7.57	12.76	1.08	3.02	0.20		0.14						0.05	0.17	20.06	10.06			95.54
KES090078	Grängesberg	Ap-veined Hm ore	in FAp		29.61			9.23	0.19	5.59	12.66	1.46	4.57	0.37		0.19		0.10	0.07				0.60	19.46	9.62			93.70
KES090079	Grängesberg	Hm-Mt ore	outside FAp		30.64			13.43	0.15	5.79	13.07	1.28	3.94	0.35		0.25		0.07			0.05		1.15	15.79	10.24			96.20
KES090083	Grängesberg	Mt-banded volcanic rock	matrix		32.66	0.56		16.33	0.55	4.93	7.66	0.75	1.96	0.35		0.29					0.06		1.67	14.41	11.59			93.76
KES090084	Grängesberg	banded impregnation of Mt+Hm in volc.	matrix		31.45			13.99	0.76	7.90	9.61	0.77	2.52	0.38		0.35		0.09					0.14	14.93	11.45			94.34
KES090088A	Grängesberg	finely banded Mt-calc-silicate	in FAp		33.10			15.47	0.26	4.19	9.36	1.04	3.80	0.51		0.38			0.08	0.05			0.51	15.92	12.03		0.05	96.74
KES090088A	Grängesberg	finely banded Mt-calc-silicate	matrix		33.22	0.12		15.29	0.21	4.64	10.14	1.10	3.78	0.44		0.28		0.08		0.12		0.05	0.64	13.10	12.14			95.33
LAL042047	Grängesberg	Mt-Hm ore	in Fe-oxide		32.56			14.70	0.51	5.27	8.64	0.81	2.72	0.49		0.24		0.16	0.05	0.07			0.53	14.78	12.30			93.83
KHO090010	Grängesberg	apatite breccia	vein infill between apatites		32.55			15.42	1.46	3.36	8.85	0.99	3.55	0.39		0.32		0.10		0.11	0.20		0.15	15.01	13.43			95.90
KHO090010	Grängesberg	apatite breccia	big crystal in matrix	0.08	31.48	0.14		14.59	0.37	5.19	11.01	1.10	4.11	0.55		0.49		0.13		0.08			0.49	14.63	9.75		0.05	94.16
KHO090011	Grängesberg	volcanic breccia	matrix	0.06	34.79	0.75		14.86	0.59	4.52	9.38	0.99	4.08	0.72		0.52		0.13		0.12			0.42	10.51	9.20		0.42	91.97
KHO090128	Grängesberg	Hm-Mt layered ore	in contact with monazite	0.10	32.87			17.01	0.08	5.46	8.57	0.49	1.38	0.09		0.12			0.06				0.32	14.66	14.88		0.05	96.03

blank - measured for, but not detected

This is a preprint, the final version is subject to change, of the American Mineralogist (MSA)
Cite as Authors (Year) Title. American Mineralogist, in press.
(DOI will not work until issue is live.) DOI: http://dx.doi.org/10.2138/am-2016-5655

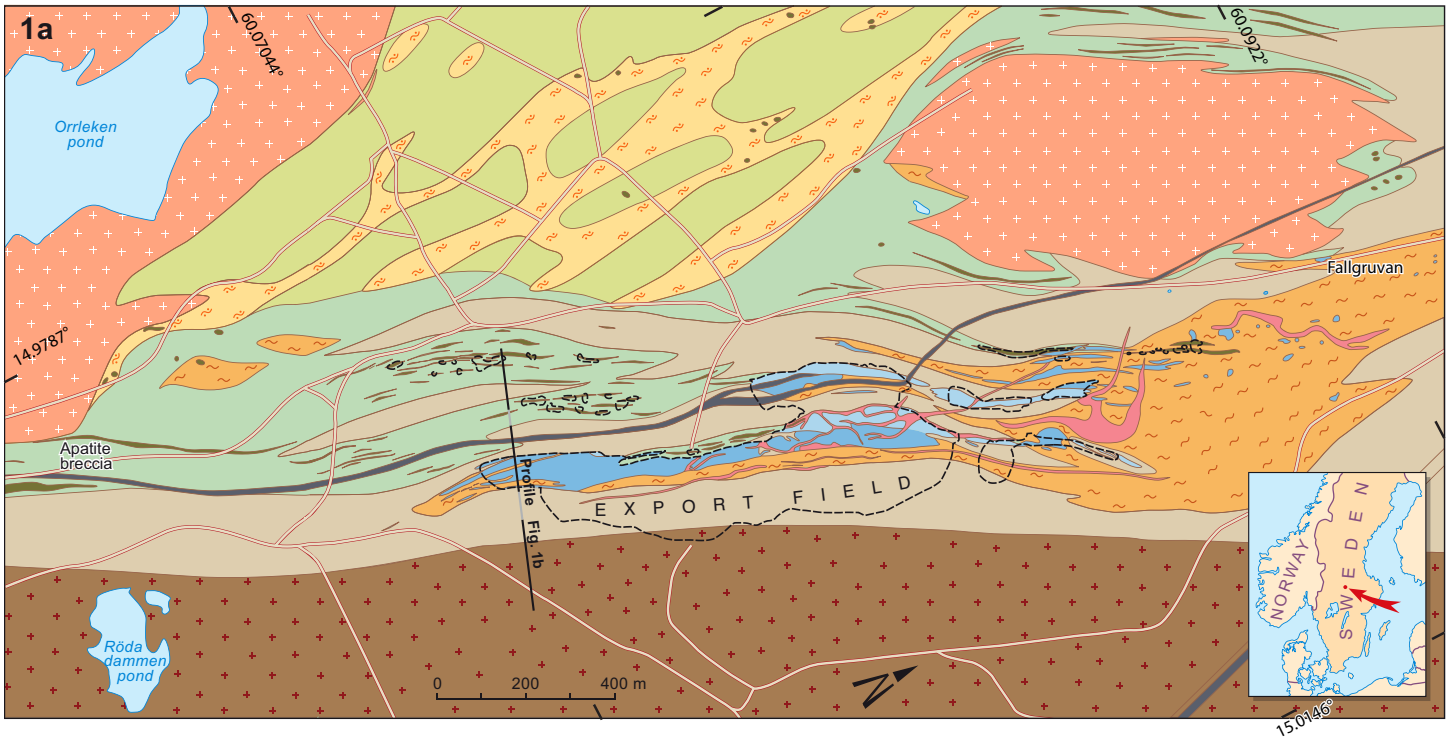

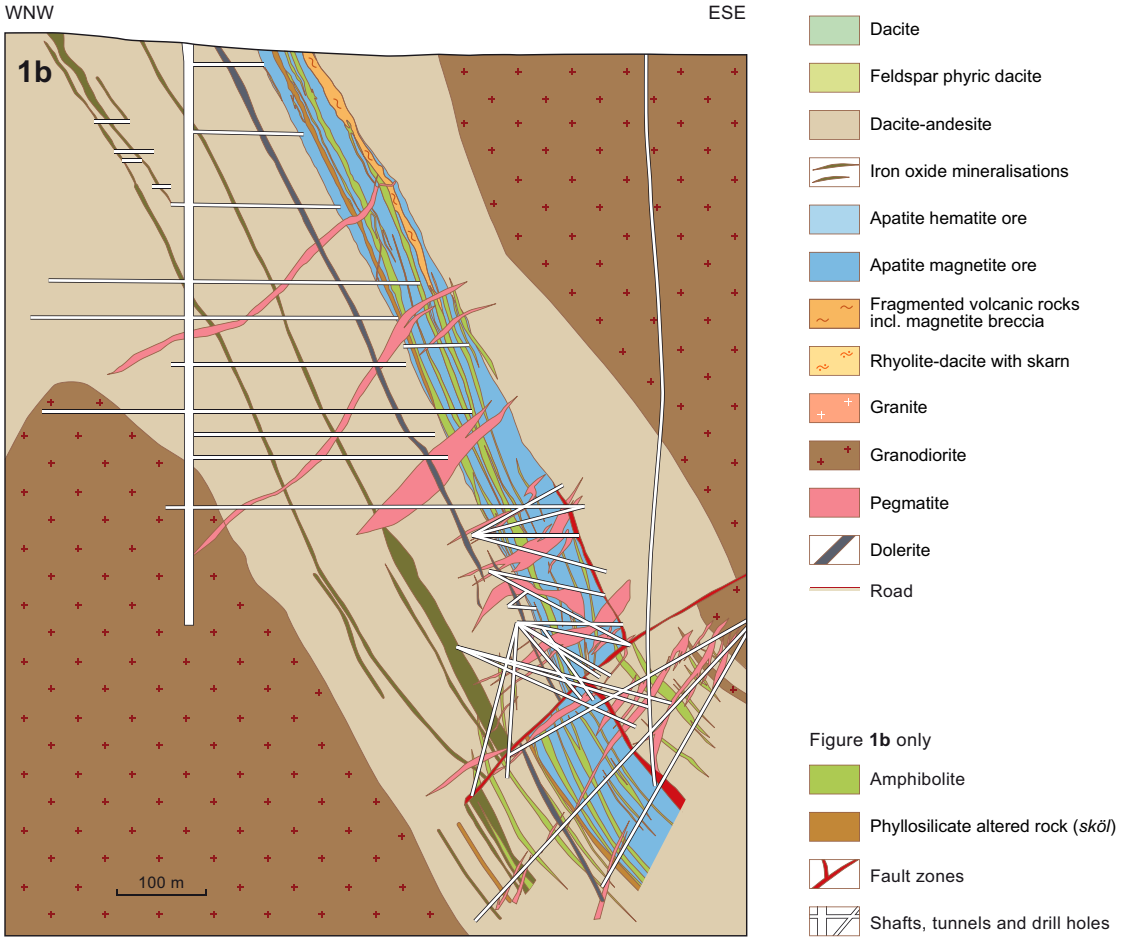

This is a preprint, the final version is subject to change, of the American Mineralogist (MSA)
Cite as Authors (Year) Title. American Mineralogist, in press.
(DOI will not work until issue is live.) DOI: http://dx.doi.org/10.2138/am-2016-5655

Figure 2

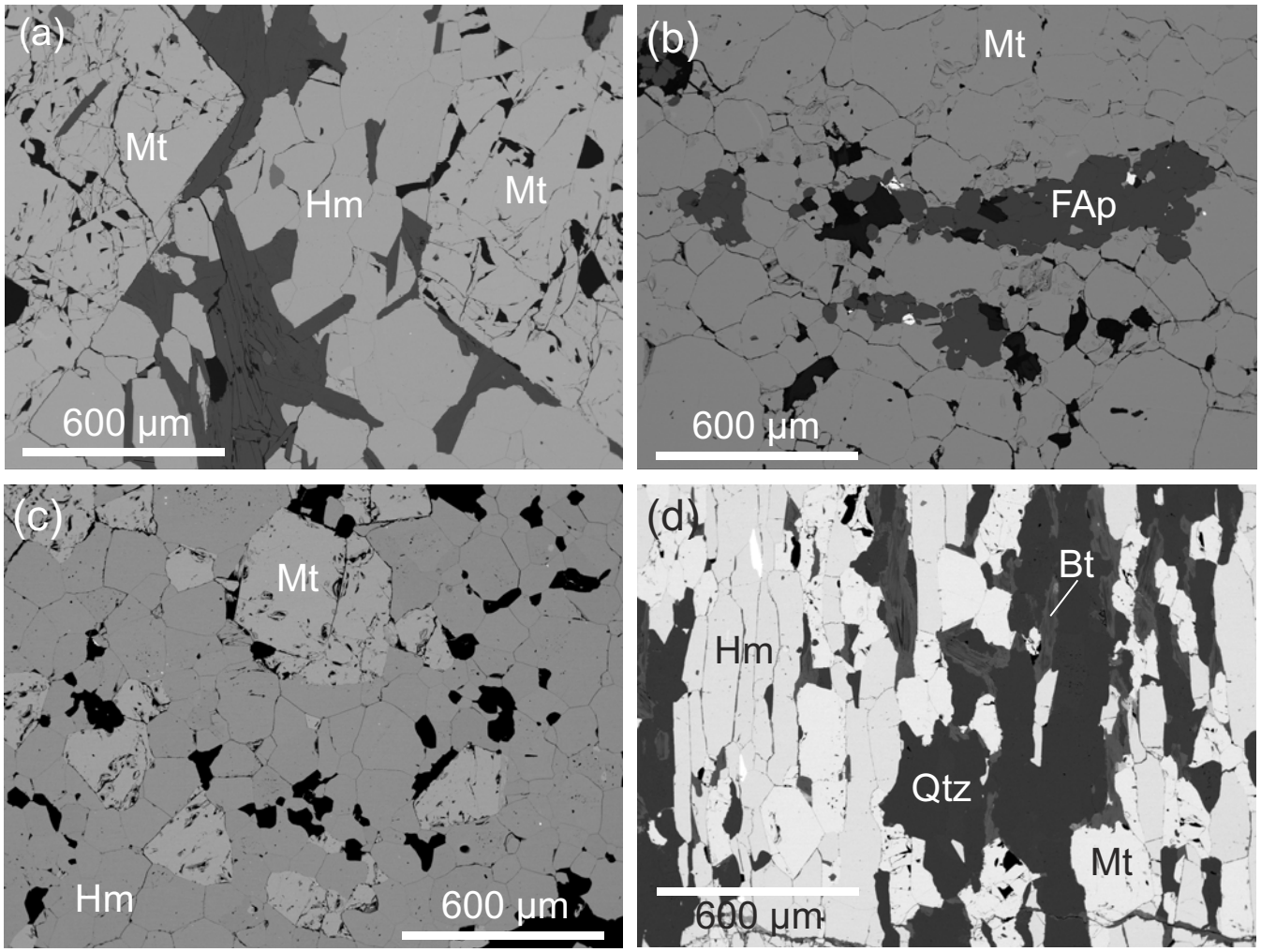

This is a preprint, the final version is subject to change, of the American Mineralogist (MSA)
Cite as Authors (Year) Title. American Mineralogist, in press.
(DOI will not work until issue is live.) DOI: http://dx.doi.org/10.2138/am-2016-5655

Figure 3

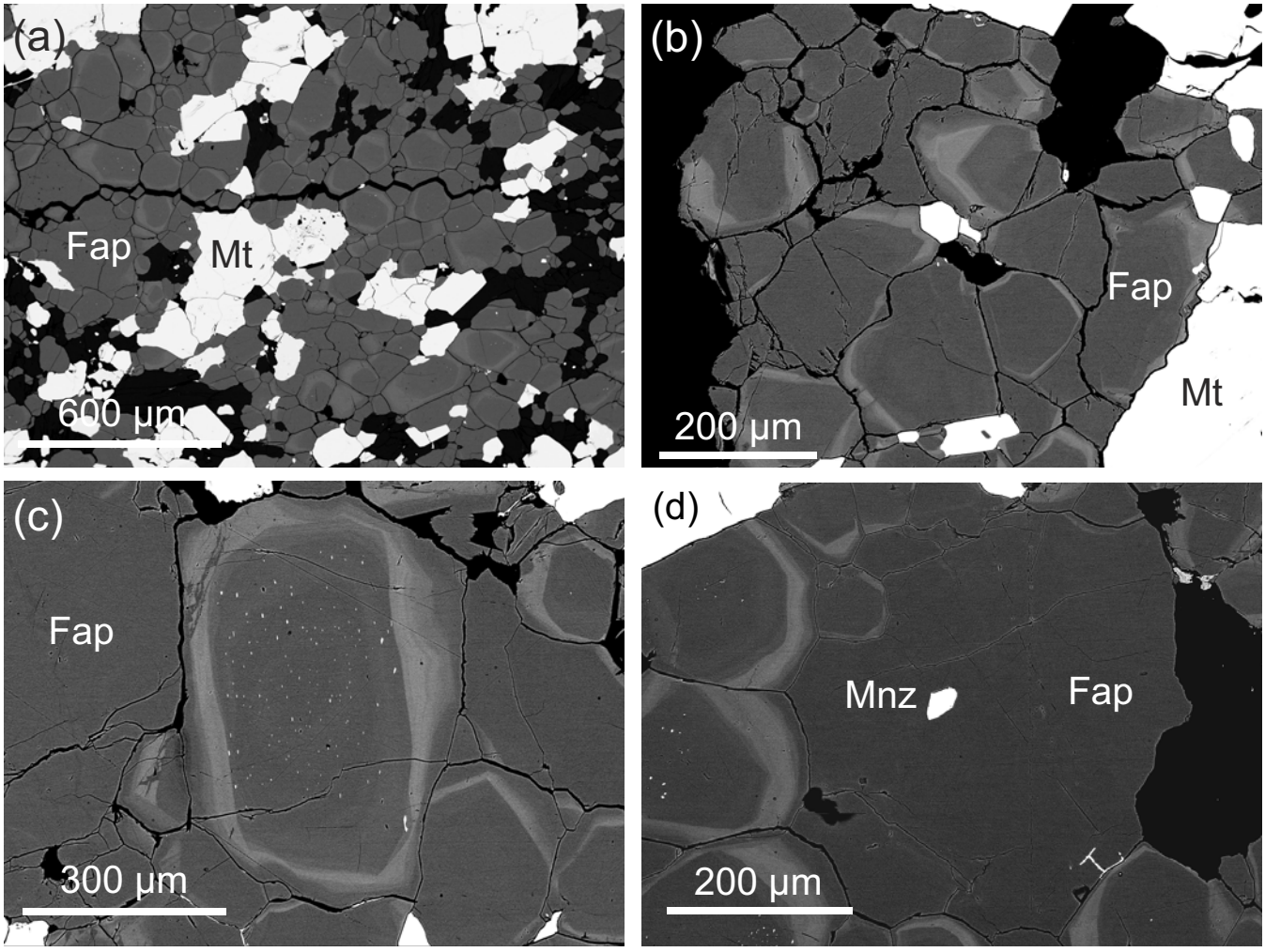

This is a preprint, the final version is subject to change, of the American Mineralogist (MSA)
Cite as Authors (Year) Title. American Mineralogist, in press.
(DOI will not work until issue is live.) DOI: http://dx.doi.org/10.2138/am-2016-5655

Figure 4

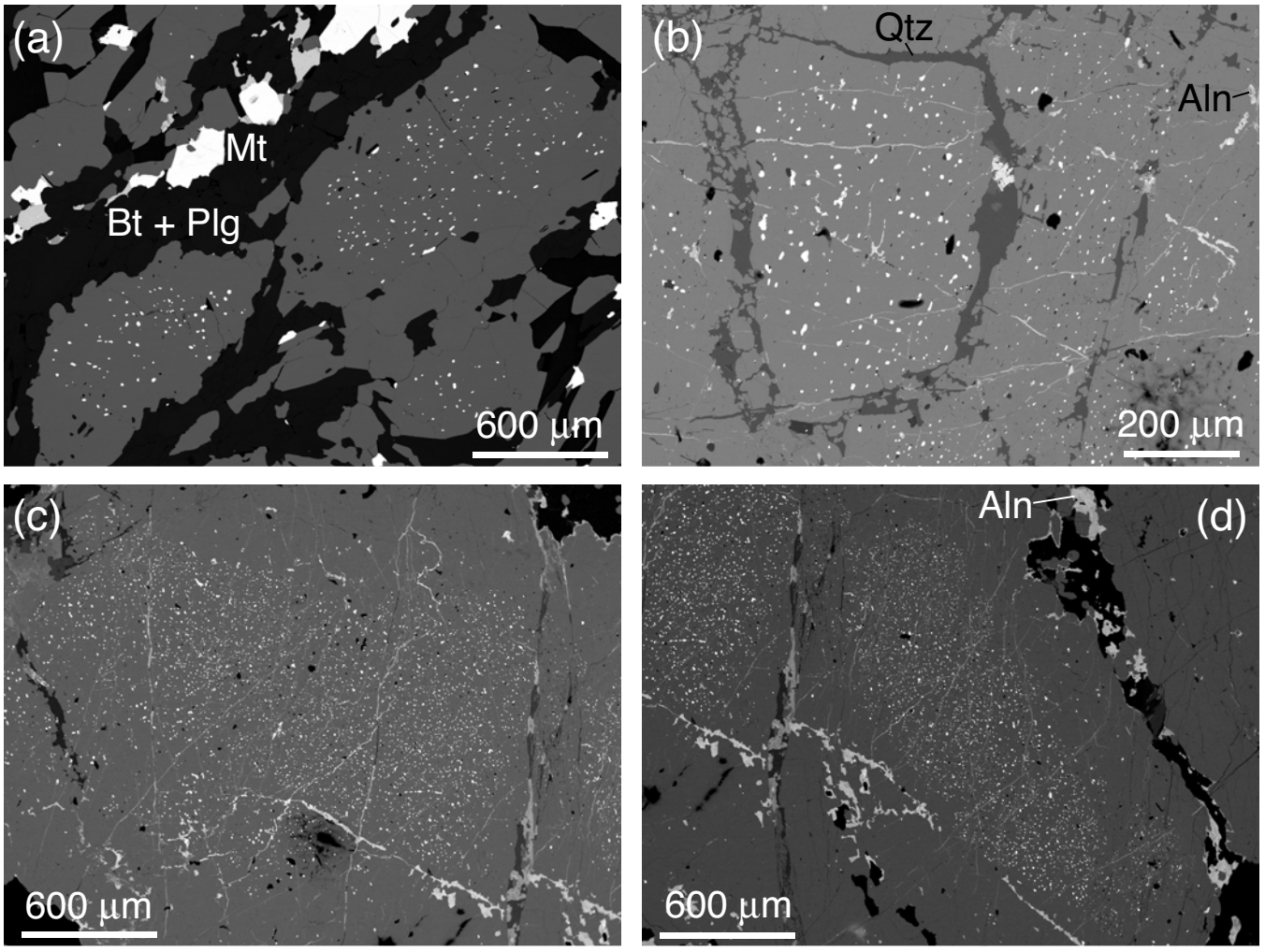

This is a preprint, the final version is subject to change, of the American Mineralogist (MSA)
Cite as Authors (Year) Title. American Mineralogist, in press.
(DOI will not work until issue is live.) DOI: http://dx.doi.org/10.2138/am-2016-5655

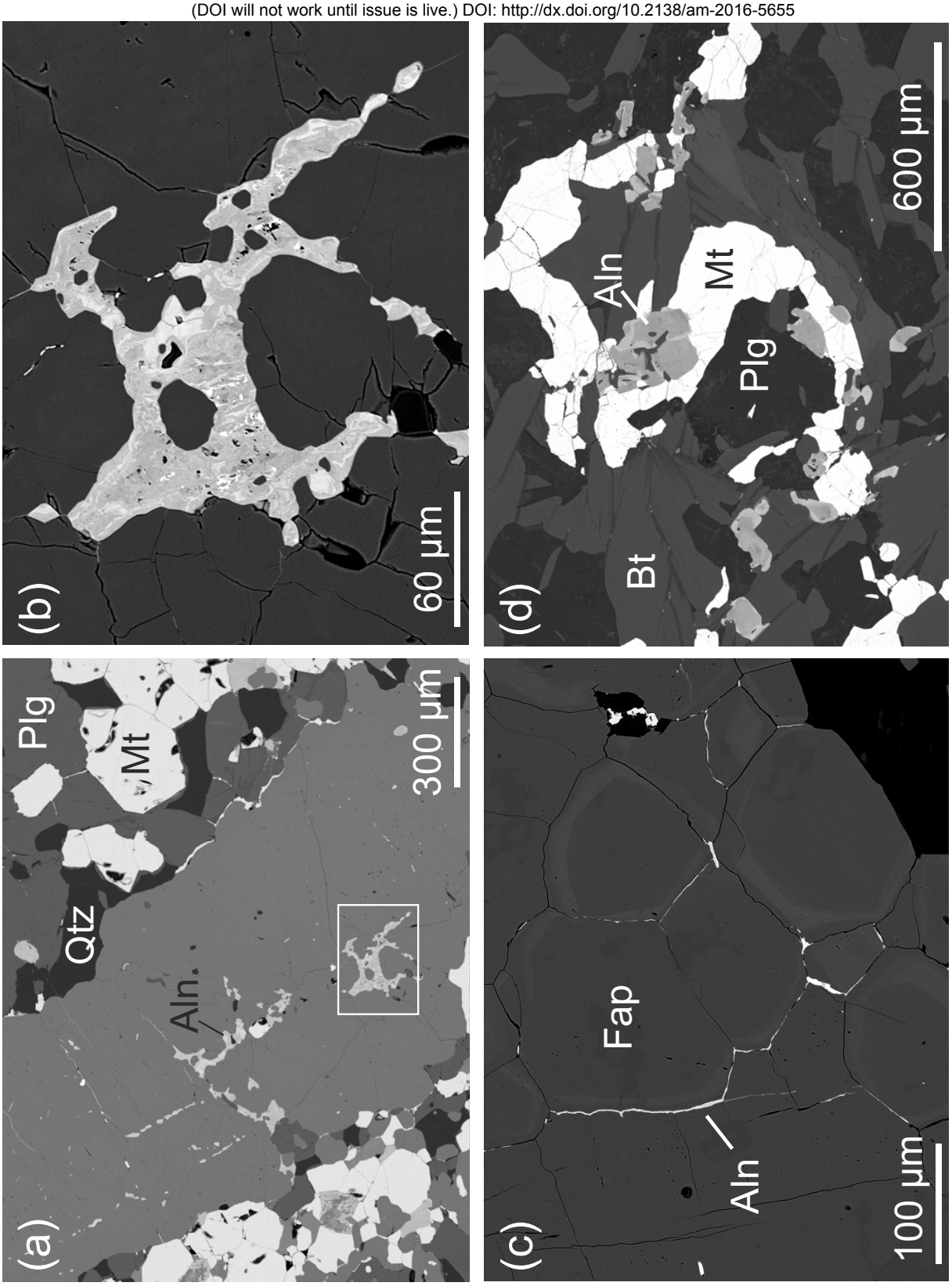

Figure 5

This is a preprint, the final version is subject to change, of the American Mineralogist (MSA)
Cite as Authors (Year) Title. American Mineralogist, in press.
(DOI will not work until issue is live.) DOI: http://dx.doi.org/10.2138/am-2016-5655

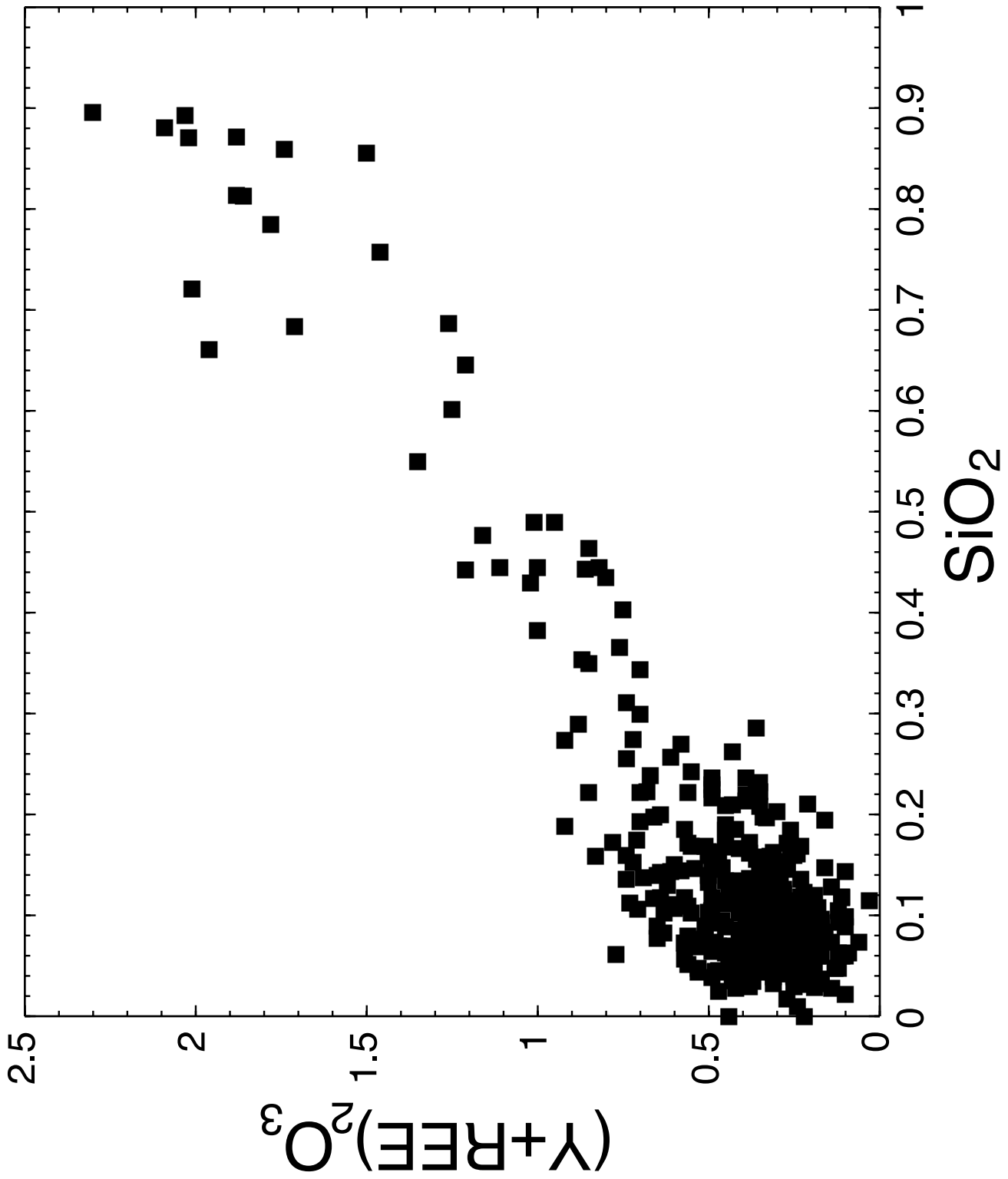

Figure 6